/rv

②

RTI

RESEARCH TRIANGLE INSTITUTE

SEMICONDUCTOR DIAMOND TECHNOLOGY

DTIC
ELECTE
DEC 3 1 1991
S
D
D

Quarterly Report -- Third Quarter
1 July 1991 - 30 September 1991

R. J. Markunas
R. A. Rudder
J. B. Posthill
R. E. Thomas

STRATEGIC DEFENSE INITIATIVE ORGANIZATION
Innovative Science and Technology Office

91-19236

91 1227 106

REPORT DOCUMENTATION PAGE
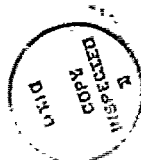
Public reporting burden for this collection of information is estimated to average 1 hour per response, including the time for reviewing instructions, searching existing data sources, gathering and maintaining the data needed, and completing and reviewing the collection of information. Send comments regarding this burden estimate or any other aspect of this collection of information, including suggestions for reducing this burden to Washington Headquarters Services, Directorate for Information Operations and Reports, 1215 Jefferson Davis Highway, Suite 1204 Arlington, VA 22202-4302, and to the Office of Management and Budget Paperwork Reduction Project (0704-0188), Washington, DC 20503

1. AGENCY USE ONLY *(Leave blank)*	2. REPORT DATE	3. REPORT TYPE AND DATES COVERED
		Quarterly Report, 1 July 1991 - 30 September 91

4. TITLE AND SUBTITLE	5. FUNDING NUMBERS
Semiconductor Diamond Technology	N00014-86-C-0460

6. AUTHOR(S)

R.J. Markunas, R.A. Rudder, J.B. Posthill, R.E. Thomas

7. PERFORMING ORGANIZATION NAME(S) AND ADDRESS(ES)	8. PERFORMING ORGANIZATION REPORT NUMBER
Research Triangle Institute P.O. Box 12194 Research Triangle Park, NC 27709	83U-3629

9. SPONSORING/MONITORING AGENCY NAME(S) AND ADDRESS(ES)	10. SPONSORING/MONITORING AGENCY REPORT NUMBER
Office of Naval Research 800 N. Quincy Street Arlington, VA 22217-5000	

11. SUPPLEMENTARY NOTES

12a. DISTRIBUTION/AVAILABILITY STATEMENT	12b. DISTRIBUTION CODE
Approved for public release; unlimited distribution	

13. ABSTRACT *(Maximum 200 words)*

The development of water-based diamond growth processes have lead to low-temperature, low-power diamond growth using water:acetic-acid:methanol mixtures. These mixtures readily inductively couple allowing low-power (500 W) inductive discharges to sustain diamond growth. Currently, growth at 300° C is possible with these acetic solutions. No serious degradation in diamond quality has been observed as the growth temperatures are reduced from 600 to 300° C..

In a parallel effort, surface chemistry studies have addressed the role of atomic O on diamond surfaces. Atomic O readily converts the 2x1 surface states into a 1x1:O terminated surfaces. Oxygen desorbs from diamond as CO at temperatures ∼ 300° C colder than atomic H desorption. Desorption of ∼ 90% of the oxygen from the surface as CO does not result in surface reconstruction. Only upon vacuum anneal to 1000° C does the diamond surface reconstruct.

14. SUBJECT TERMS	15. NUMBER OF PAGES
	67
	16. PRICE CODE

17. SECURITY CLASSIFICATION OF REPORT	18. SECURITY CLASSIFICATION OF THIS PAGE	19. SECURITY CLASSIFICATION OF ABSTRACT	20. LIMITATION OF ABSTRACT
UNCLASSIFIED	UNCLASSIFIED	UNCLASSIFIED	

TABLE OF CONTENTS

Accesion For		
NTIS CRA&I	☑	
DTIC TAB	☐	
Unannounced	☐	
Justification		
By		
Distribution /		
Availability Codes		
Dist	Avail and / or Special	
A-1		

1.0 SUMMARY OF PROGRESS

This is the 1991 Third Quarterly Report on the Semiconducting Diamond Program Contract No. N-00014-C-0138 at Research Triangle Institute. Work on the diamond program during this quarter found new directions as the water-based diamond growth process became a generic deposition process in our laboratory. (A letter was submitted to Applied Physics Letters describing the water-alcohol vapor growth. A copy of the submission is included in this quarterly report.) Surface chemistry experiments began to address the role of O on the diamond (100) surface. It was found that unlike atomic hydrogen atomic O readily converts the 2×1 surface to a 1×1 oxygen stabilized surface. The conversion occurs for near monolayer doses of atomic oxygen. (A presentation was given at the American Vacuum Society Meeting disclosing these results. The subsequent paper was submitted to the Journal of Vacuum Science and Technology as part of the conference proceedings. A copy is included in this quarterly report.) Interest in the water-based processing continued to heighten as organic acids were added to the water solutions. Acetic acid addition to the water-based process reduced the temperature and power requirements for diamond growth.

2.0 SURFACE CHEMISTRY (See Attached Article)

4

Thermal Desorption from Hydrogenated and Oxygenated Diamond (100)
Surfaces.

R.E. Thomas, R.A. Rudder, and R.J. Markunas

Research Triangle Institute, Research Triangle Park. NC 27709

ABSTRACT

Low energy electron diffraction (LEED) has been used to study the effects of atomic and molecular species of hydrogen and oxygen on the reconstructed C(100)-(2x1) surface. Thermal desorption spectroscopy was also used to study desorption products and kinetics from hydrogenated and oxygenated surfaces. Atomic hydrogen appears relatively inefficient at breaking C-C dimer bonds on the (100)-(2x1) surface. Atomic oxygen, in contrast, readily converts the surface from the 2x1 state to the 1x1 state. This process is reversible for a limited number of cycles before degradation of the surface obscures the 2x1 LEED pattern. Oxygen is thought to adsorb in one of two configurations, bridging carbon atoms on the surface, or double bonded to a single carbon atom on the surface.

Thermal desorption of molecular hydrogen from hydrogenated C(100)-(2x1):H surfaces occurs at approximately 900° C for a heating rate of 20° C/s. Molecular hydrogen is the major desorption product and the desorption temperature appears to be coverage independent. Thus the desorption kinetics are most likely first order. Thermal desorption of carbon monoxide from oxygenated C(100)-(1x1):O surfaces occurs at approximately 600° C for a heating rate of 20° C/s. Carbon monoxide is the major pro-

duct seen, with small quantities of carbon dioxide also observed. For increasing oxygen coverages, the desorption peak is observed to shift to lower temperatures. A peak shift to lower temperatures can be interpreted as either first order kinetics with a coverage dependent activation energy or second order kinetics. The reaction order is not known in this case, but from analysis of the peak shapes and from the fact that CO can desorb without prepairing, the data suggest that the reaction is first order.

I. INTRODUCTION

Hydrogen plays an integral role in many of the CVD diamond growth processes developed to date.[1] Hydrogen is thought to function in the growth process in a number of ways, including maintenance of sp^3 hybridization of carbon atoms at the growth surface. Oxygen has been used in concentrations of approximately 1-2% in H_2/CH_4 plasmas to extend the diamond growth regime with respect to gas composition and substrate temperature.[2,3] The role oxygen plays is perhaps more complicated. It has been suggested that oxygen increases the atomic hydrogen concentration through gas phase reactions and also etchs non-diamond carbon.[2] Recently, however, oxygen has been introduced to the growth process in much larger concentrations in the form of water and alcohols.[4] Bachmann et al. have assembled data from a variety of growth techniques to produce an empirical H-C-O diamond growth phase diagram.[16] The diagram indicates that diamond can be successfully grown with carbon and oxygen alone. In spite of numerous growth studies, the details of the roles of hydrogen and oxygen in the CVD growth environment are still unclear, as are fundamental questions concerning interactions of these two gasses with the diamond surface. In order to greatly simplify the systems under consideration, we have used a combination of low pressure gas dosing and temperature programmed desorption to study interactions of relatively simple gasses such as atomic hydrogen and atomic oxygen with a clean diamond surface.

Although similar in structure to the silicon (100) surface, the diamond (100) surface has not been studied nearly as intensively, with only a handful of experimental

studies published to date.[5,6,7,8,9] Important questions remain concerning the details of the reconstruction and the effect of adsorbates on surface structure. As with silicon (100) the diamond (100) surface reconstructs to a rotated 2x1 dimer configuration upon heating.[5,7,9] Due to the higher bond strengths in the carbon system the reconstruction does not occur until the diamond is annealed to approximately 1000°C, as opposed to 450°C for silicon. There is also evidence that the reconstruction is not necessarily coupled with the thermal desorption of hydrogen from the surface as in the case of silicon. Hamza et al report that both thermal desorption signals and "fast" protons generated by electron stimulated desorption are eliminated below 925°C.[5] However, they report that the LEED half-order spot intensity does not begin to appear until the sample is annealed at 965°C.[5]

Adsorption of atomic hydrogen has been reported to convert the surface back to the 1x1 configuration.[5] However, subsequent annealing to 1200° C did not convert the surface back to the 2x1 configuration.[5] Theoretical calculations indicate a substantial barrier for the insertion of hydrogen into the C-C dimer bond.[10,11,17] From these calculations it appears difficult to form the dihydride from the monohydride by the exposure of the 2x1 surface to atomic hydrogen at 25°C.

Oxygen interactions with the (100) surface are less well studied than those of hydrogen. Lurie and Wilson report no observable effect on LEED patterns upon exposure of the (100) surface to molecular oxygen.[9] Matsumoto exposed diamond powder to molecular oxygen at atmospheric pressure and room temperature and at 1 Pa at 500°C.[12] In the case of the powder desorption, CO desorption peaks were seen at

approximately 600°C. Smaller desorption peaks were seen for CO_2 at approximately 500°C.

In the present paper we have used LEED to study the effects of atomic and molecular species of hydrogen and oxygen on the reconstructed 2x1 surface. Thermal desorption spectroscopy was also used to study desorption products and kinetics from hydrogenated and oxygenated surfaces.

II. EXPERIMENTAL PROCEDURES

Thermal desorption spectroscopy and LEED observations were performed in a stainless steel UHV system shown in Figure 1. Turbomolecular pumps were used both on the main chamber and to differentially pump the chamber housing the quadrupole mass spectrometer. Additional hydrogen pumping capacity for the quadrupole chamber was provided by a bulk getter pump. Base pressure was 5×10^{-10} Torr for the sample chamber and 1×10^{-10} Torr for the quadrupole chamber. The sample chamber was separated from the quadrupole chamber by a 2mm diameter stainless steel aperture.

Sample heating was accomplished by clipping the crystals to a 0.25mm thick molybdenum resistive strip heater. (inset Fig. 1) All parts associated with the heater stage, including the clamps and current leads were manufactured from molybdenum. The sample temperature was measured by a 0.125mm diameter chromel/alumel thermocouple threaded through a laser drilled hole in the diamond and held in tension against the crystal. (inset Fig. 1) Sample heating was controlled by feedback from the thermocouple to a SCR power supply. After an initial warm-up phase, temperature

ramps are linear from approximately 150°C to over 1100°C.

A series of control experiments were performed to ensure that thermal desorption signals observed actually originated from the sample surface. For both atomic hydrogen and atomic oxygen, samples were dosed in the standard manner and thermal desorptions run with the sample either adjacent to, but not in front of, the aperture, or with the aperture centered on a portion of the sample mounting assembly. No thermal desorption peaks were observed in any of the control experiments.

Two type IIa (100), 5x5x0.25mm, diamond crystals were used in the course of the present study. Other than thermal cleaning, no technique is available in situ for removing surface contamination from the diamond crystals. Particular attention was therefore paid to preparing the diamond surface before mounting in the vacuum system. The samples are initially hand polished for 5 minutes with 0.25μm diamond grit and deionized water on a nylon polishing pad. The samples are then ultrasonically degreased in a series of solvents, trichloroethylene, acetone, methanol, and deionized water. Following the deionized water rinse, the samples are swabbed under DI water to remove particles. The samples are rinsed again in the solvent series and then placed in CrO_3/H_2SO_4 (125°C) solution for 20 minutes to remove non-diamond carbon. The samples are rinsed in DI water and then boiled in a 3:1 solution of HCl/HNO_3 for 20 minutes to remove any metals contamination. Finally the samples are rinsed in deionized water and blow-dryed with compressed nitrogen. Samples subjected to this cleaning process typically show a good quality 1x1 LEED pattern with no annealing. For the initial thermal cleaning the samples were ramped up in temperature at approxi-

mateiy 10°C/sec until the pressure in the main chamber rose to 5×10^{-8} Torr at which point the power was shut off and the samples cooled. This cleaning cycle continued until a maximum temperature of 1150°C was reached.

In all cases atomic hydrogen was generated via a tungsten filament operating at a temperature of approximately 1500°C. The sample was positioned approximately 2 cm. from the filament during dosing. The sample was not actively cooled and at the lowest dosing pressures remained at room temperature. Atomic oxygen was generated via an iridium filament at 1100°C. VLSI grade hydrogen and oxygen gasses were used with no further purification. No attempt was made to quantify the percentage of atomic species generated by the filaments. All doses are given for the total H_2 and O_2 exposure from uncorrected ion gauge tube readings. X-ray photoelectron spectroscopy was done ex situ after extensive dosing with both the tungsten and the iridium filaments and no evidence of metals contamination was seen.

III. EXPERIMENTAL RESULTS

A. Hydrogen dosing studies

Upon annealing more than 90% of the freshly polished surfaces used in the present study exhibited a transformation from the 1x1 configuration to the 2x1 configuration. During the initial annealing sequence the samples would typically show indications of the 2x1 structure at approximately 800°C, with the transformation completed by 1050°C on successive anneals. No correlations were observed between sample preparation conditions and failure of the surface to reconstruct.

Initial studies were concerned with exposure of the reconstructed diamond surface to atomic hydrogen. We find that even after extensive dosing with atomic hydrogen the surface remains in a 2x1 configuration. The maximum dose the samples received was approximately 40000L(H/H$_2$). In contrast, a dose of 600L under identical conditions is sufficient to convert the silicon (100) surface from the 2x1 state back to the 1x1 state. Given that we were unable to convert the surface back to the 1x1 configuration with atomic hydrogen, the subsequent adsorption and desorption experiments were all performed on the 2x1 surface.

In the next series of experiments clean 2x1 surfaces were dosed with varying quantities of atomic hydrogen and thermal desorption spectra were recorded. The primary desorption product observed was molecular hydrogen at approximately 900°C. Figure 2 shows a series of desorption spectra taken after increasing atomic hydrogen exposures. There is no evidence of a shift in desorption peak temperature as a function of coverage, indicating the desorption process is first order. Exposure of the clean surface to equivalent doses of molecular hydrogen with no heated filament gave no thermal desorption features. Figure 3 shows a plot of integrated H$_2$ desorption peak area versus hydrogen dose. We can see that uptake for the surface is not linear with dose and that the surface appears to approach saturation while still in the 2x1 configuration. In addition to monitoring hydrogen, masses 12-18, 26-32, and 44 were scanned in the course of the experiments. Small quantities of masses 15, and 26 were observed to desorb from the surface but contamination from the source gas can not be ruled out at this time.

B. Oxygen dosing results

Exposure of a reconstructed 2x1 surface to a mixture of atomic and molecular oxygen results in conversion of the surface to the 1x1 state. Exposure of an identical surface to a molecular oxygen dose an order of magnitude larger has no apparent affect on the surface structure, the LEED remains in a 2x1 pattern. Annealing of the 1x1:O surfaces to 1000°C results in the restoration of the 2x1 surface. The cycle can be repeated approximately 10-15 times before the LEED is left with weak first order spots only and a very high background. It should be emphasized that the surface is etched during each CO desorption cycle which may lead to roughening of the surface and deterioration of the LEED pattern.

Figure 4 shows a series of thermal desorption spectra for mass 28 (CO) from a diamond surface. The desorption traces show very broad peaks with a maximum in the desorption rate at approximately 600°C. We also see a shift to lower desorption temperatures as coverage increases. Figure 5 snows the integrated area under the desorption peaks plotted as a function of total oxygen exposure. The sample shows a steep initial uptake followed by a much slower uptake at the higher exposures. The sample does not completely saturated after a dose of 4500L although the uptake does decrease markedly.

In addition to mass 28, masses 2,16,17,18,32, and 44 were monitored. Small amounts of mass 44 were observed and were presumed to arise from CO_2. Figure 6 shows a comparison of the mass 44 thermal desorption and the mass 28 from the same desorption experiment. Note that the vertical scale for mass 44 has been expanded by

a factor of 4. The maximum desorption rate occurs at approximately 550°C for both masses but the CO_2 peak is much more asymmetric than the CO peak.

IV. DISCUSSION

Reconstruction of the diamond (100) surface to the 2x1 state is a well documented phenomena.[5,6,7,9] However, most researchers report that a percentage of the freshly polished surfaces studied do not reconstruct to the 2x1 structure upon annealing. Hamza et al. have reported an association between residual oxygen on the surface detected by electron stimulated desorption and the ability of the surface to reconstruct.[5] Samples with the most oxygen detected were less likely to reconstruct. Given the surface preparation techniques available (both in situ and ex situ) for diamond, it seems reasonable to assume that surface contamination may explain the failure of some samples to reconstruct. The effect of impurities on surface reconstruction has been noted in a number of other systems including silicon and platinum.[13]

Conversion of the surface back to the 1x1 state by exposure to atomic hydrogen has been studied in detail by only one other group.[5] Results reported by Hamza et al. indicated that the surface converted to the 1x1 configuration upon dosing with atomic hydrogen at 180K coupled with annealing at 700K.[5] LEED patterns disappeared following the dosing and the 1x1 pattern was then seen after annealing.[5] We see no evidence of either obscuration of the LEED pattern following dosing or of a reversion to the 1x1 surface structure. The LEED patterns gradually deteriorated with repeated dosing and desorption cycles until only weak first order spots remained coupled with a very high background. One expects the dimer bond on the C(100)-(2x1) surface to be

14

stronger than what is seen on the Si(100)-(2x1) surface given the greater C-C bond strength, 83 kcal/mol versus 46 kcal/mol for Si-Si, and the ability of carbon to form double bonds. Calculations of hydrogen addition to the 2x1 surface by several groups indicates that there is an energy barrier to the breaking of the dimer bond by the addition of atomic hydrogen.[10,11,17] Verwoerd[10] calculates an energy barrier of approximately 39 kcal/mol), an energy barrier of 34.1 kcal/mol was estimated by Zheng, and Smith[11], and 48.7 kcal/mol by Thomas et al.[17] Yang and D'Evelyn have argued that steric constraints severely limit the ability of the surface to saturate in the dihydride phase, and at most the surface assumes a disordered dihydride with random dihydride units scattered among monohydride pairs.[14] Based on these results it appears unlikely that adsorption of atomic hydrogen at room temperature will result in a conversion to the dihydride state.

As noted above, since we were unable to obtain a 1x1 structure by hydrogen adsorption, all desorption results discussed here are from a 2x1 surface. We see no evidence of a peak shift with respect to surface coverage to within the resolution of the measurement, (10 °C). The lack of a peak shift argues for first order desorption kinetics. Application of the rate equation with an assumed frequency factor of 10^{13}/s gives 72.7kcal/mol for the activation energy of desorption.

Oxygen behaves in a very different fashion than hydrogen on the diamond surface. The most dramatic difference is the apparent ability of atomic oxygen to break the C-C dimer bonds on the surface. We have no effective method of monitoring products formed during dosing as a result of atomic oxygen interactions with the diamond

15

surface. As such, the oxygen may be etching the C-C dimers from the surface and then attaching oxygen atoms to the bulk crystal structure. The other case of course is for oxygen to attack the dimers directly and break the dimer bond.

Once the oxygen has attached to the surface there are several possible bonding configurations. The oxygen could bridge two adjacent carbon atoms with a single bond to each, as shown in Figure 7. Table 1 shows the bond angle oxygen would have to assume in the bridging configuration. At 125°, the angle is well within the range of bond angles that oxygen assumes in various molecules. In order to calculate the bond angle the C-O bond length was taken as 1.43Å and the separation distance between the two carbon atoms that the oxygen bridges was taken as 2.52Å. Another possibility is for each oxygen to double bond to a single carbon as shown in Figure 7. One would expect 1x1 LEED patterns from both of these bonding configurations so it may be difficult to distinguish between the two cases on the basis of qualitative electron diffraction. Based on the models described above, oxygen should exhibit very different behavior on the diamond (111) surface.

Results from thermal desorption experiments indicated that as the coverage increased the temperature for the maximum CO desorption rate decreased. This can be interpreted as either a first order desorption with a coverage dependent activation energy or a second order desorption process. One might expect desorption of CO from the surface to be first order rather than second order as there is no requirement for pairing of atoms prior to desorption. For a first order process we would expect to see an asymmetric peak with the high temperature side of the peak more steeply sloped.

In fact the asymmetry appears to be in the opposite direction with the high temperature side of the peak less steeply sloped than the low temperature side. One explanation for the asymmetry may be additional peaks on the high temper. .⁻ side of the main peak. A slower heating rate, perhaps 1°C/sec may resolve an ..)..⁻. ..⁻ peaks which may be present. Supporting evidence for additional CO peaks above 600°C comes from powder desorption work done by Matsumoto.[12] Matsumo' . ' as measured oxygen desorption from diamond powders exposed to molecular oxygen at temperatures between 420°C and 554°C.[12] Adsorption was done at a pressure of 1 Pa. CO peaks are seen at 600°C and 800°C for heating rates of 20°C/min. A smaller CO_2 peak is seen at approximately 500°C. The heating rate used by Matsumoto et al. is a factor of 60 slower than the rate used in the study reported here. One might expect the peak to shift down in temperature as a result of the slower heating rate.

The peaks seen for CO desorption are very broad, with a FWHM of approximately 350°C for the highest coverages. Hydrogen desorption peaks in contrast had a FWHM of about 100°C. Part of the peak width may be explained if in fact there are additional peaks in the CO desorption curves. Relatively broad CO desorption peaks, FWHM approximately 300°C, are also observed from from oxygen dosed single crystal graphite surfaces.[15] It is interesting that two peaks, 800°C and 1000°C, were recorded from these surfaces.

V. CONCLUSIONS

Thermal mass desorption and LEED have been used to study and contrast atomic hydrogen and atomic oxygen interactions with the diamond(100)-(2x1) surface. Atomic

17

hydrogen appears relatively inefficient at breaking C-C dimer bonds on the (100)-(2x1) surface. Atomic oxygen, in contrast, readily converts the surface from the 2x1 state to the 1x1 state. This process is reversible for a limited number of cycles before degradation of the surface obscures the 2x1 LEED pattern. Oxygen is thought to adsorb in one of two configurations, bridging carbon atoms on the surface. or double bonded to each carbon atom on the surface.

Thermal desorption from hydrogenated C(100)-(2x1):H surfaces occurs at approximately 900°C for a heating rate of 20°C/s. Molecular hydrogen is the major desorption product and the desorption temperature appears to be coverage independent. Thus the desorption kinetics are most likely first order. Thermal desorption from oxygenated C(100)-(1x1):O surfaces occurs at approximately 600°C for a heating rate of 20°C/s. Carbon monoxide is the major desorption product seen, but small quantities of carbon dioxide were also observed. For increasing oxygen coverages, the desorption peak is observed to shift to lower temperatures. The reaction order is not known in this case, but from analysis of the peak shapes and from the fact that CO can desorb without prepairing, the data suggest that the reaction is first order. Clear differences exist between the behavior of hydrogen and oxygen on the diamond (100) surface. Oxygen is able to convert the 2x1 surface back to the 1x1 configuration whereas hydrogen appears relatively inefficient at this process. Although the dosing studies were performed at room temperature the results may help to explain the role of oxygen in H_2/CH_4 growth environments. If surface dimers form during the growth process it appears that atomic hydrogen is relatively inefficient at breaking the dimer bonds.

Atomic oxygen appears to restore the surface much more efficiently than atomic hydrogen.

Acknowledgements

TABLE I

Bonding Angles of Oxygen

Molecule	Bond Angle	Bond Length (angstroms)	
water	104°	O-H	.96
α-quartz	144°	O-Si	1.6
methyl ether	110°	O-C	1.43
diamond	125°	O-C	1.43(assumed)

REFERENCES

1. See references in "Proceedings of the Second International Conference on New Diamond Science and Technology", edited by R. Messier, J.T. Glass, J.E. Butler, and R. Roy (Materials Research Society, Pittsburgh, PA, 1991).

2. J.A. Mucha, D.L. Flamm, and D.E. Ibbotson, J. Appl. Phys. 65 3448 (1989).

3. S.J. Harris, and A.M. Weiner, Appl. Phys. Letts. 55, 2179 (1989).

4. R.A. Rudder, G.C. Hudson, J.B. Posthill, R.E. Thomas, R.C. Hendry, D.P. Malta, R.J. Markunas, T.P. Humphreys, and R.J. Nemanich, to be published, Appl. Phys. Lett.

5. A.V. Hamza, G.D. Kubiak, and R.H. Stulen, Surf. Sci. 237, 35 (1990).

6. B.B. Pate, Surf. Sci. 165, 83 (1986).

7. R.E. Thomas, R.A. Rudder, and R.J. Markunas, "Thermal Desorption From Hydrogenated Diamond (100) Surfaces", presented at 179th meeting of The Electrochemical Society, Wash, DC, May 1991. To be published, Conf. Proc.

8. J.P.F. Sellschop, C.C.P. Madiba, and H.J. Annegarn, Nucl. Instrum. Meth. 168, 529 (1980).

9. P.G. Lurie, and J.M. Wilson, Surf. Sci. 65, 453 (1977).

10. W.S. Verwoerd, Surf. Sci. 108, 153 (1981).

11. X.M. Zheng, and P.V. Smith, Surf. Sci. 256, 1 (1991).

12. S. Matsumoto, and N. Setaka, Carbon 17, 485, (1979); S. Matsumoto, Y. Sato, and N. Setaka, Carbon 19, 232, (1981).

13. A. Zangwill, *Physics at Surfaces*, (Cambridge University Press, Cambridge, England, 1988), pp. 96, 258.

14. Y.L. Yang, and M.P. D'Evelyn, submitted to J. Am. Chem. Soc.

15. B. Marchon, J. Carrazza, H. Heinemann, and G.A. Somorjai, Carbon 26 507 (1988).

16. P.K. Bachmann, D. Leers, and H. Lydin, Diamond and Related Materials 1 1 (1991).

17. R.E. Thomas, R.A. Rudder, R.J. Markunas, D. Huang. and M. Frenklach, submitted for publication, J. Chem. Vapor Deposition.

Figure Captions

Figure 1. Schematic view of system. Inset in this figure is a drawing showing details of the sample mounting and heater geometry.

Figure 2. Thermal desorption spectra from hydrogenated diamond-(2x1) surfaces. Molecular hydrogen was the major desorption product observed from all surfaces dosed with atomic hydrogen. All dosing was performed at 25°C. Samples were exposed to a mixture of H and H_2 produced by the tungsten filament.

Figure 3. Plot of H_2 integrated peak area versus total dose H/H_2. The peak areas were normalized to the largest H_2 area measured.

Figure 4. Thermal desorption spectra showing CO desorption from oxygen dosed diamond surfaces. Samples were exposed to a mixture of O and O_2 after molecular oxygen was passed over an iridium filament.
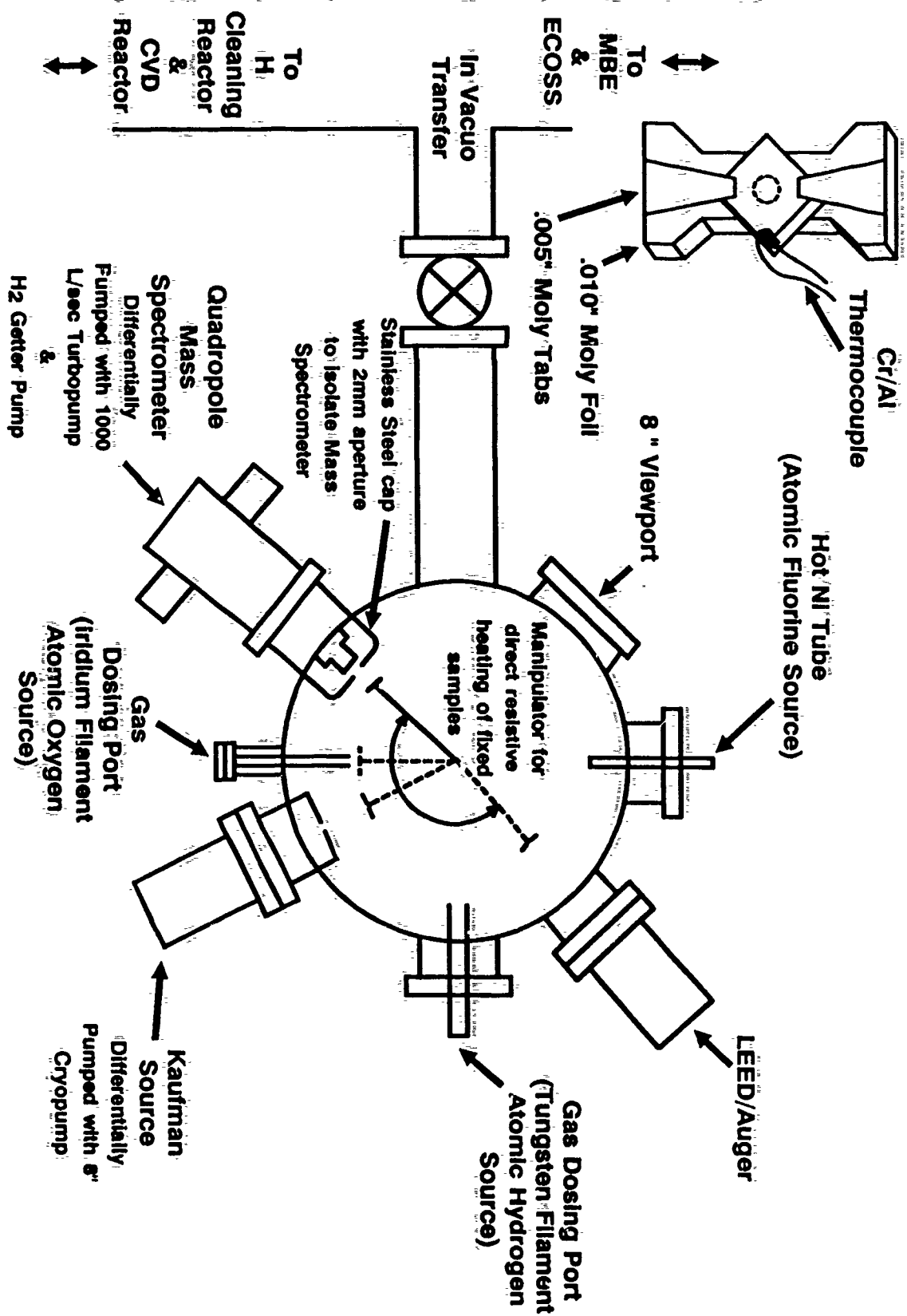
Figure 5. Plot of CO integrated peak area versus total dose of O/O_2. As in Fig. 3, the peak ares were normalized to the largest CO peak area measured.
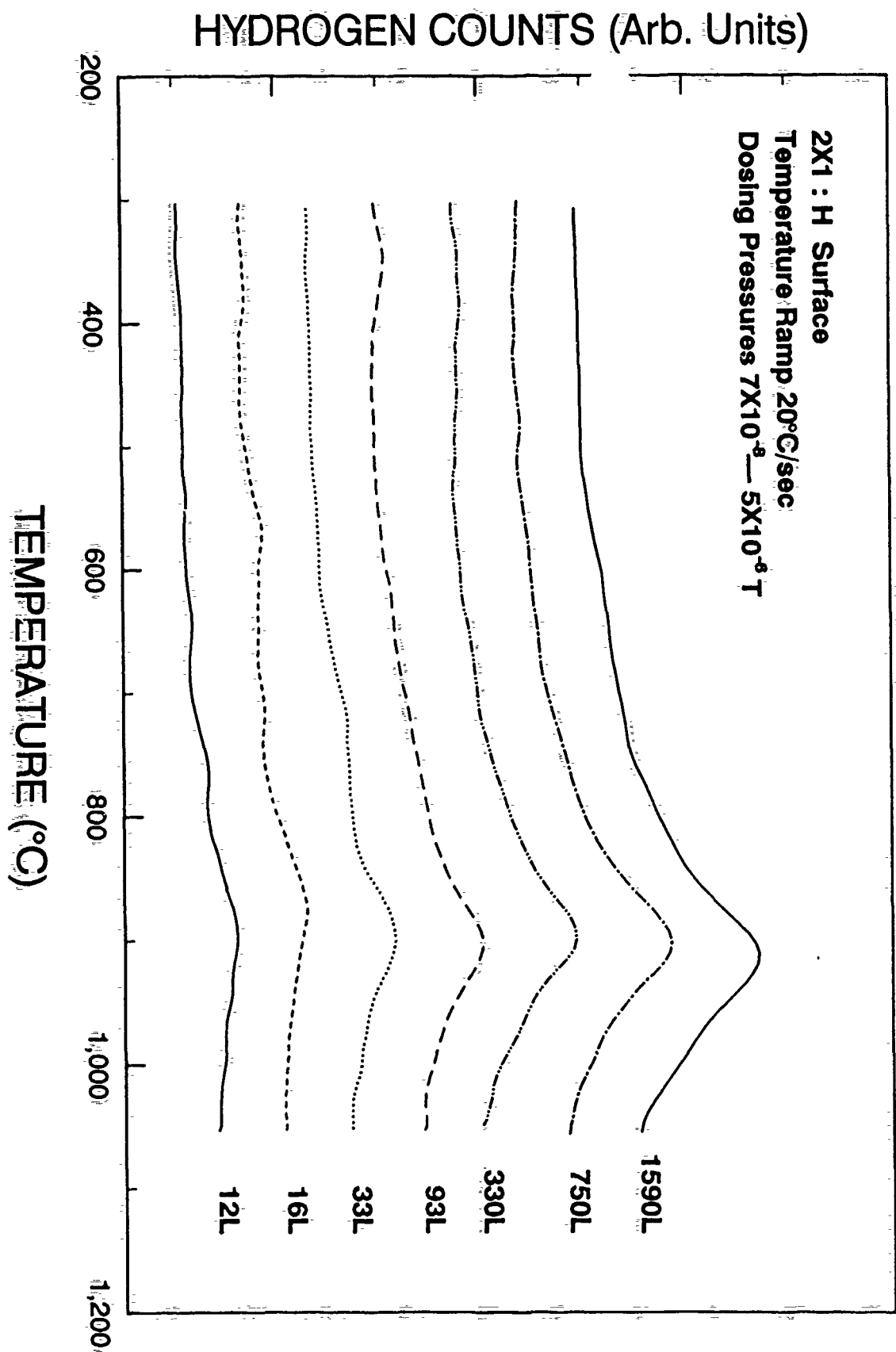
Figure 6. This desorption spectrum shows both mass 28 (CO) and mass 44 (CO_2) as taken simultaneously from an O/O_2 dosed sample. The mass 44 vertical scale has been expanded by a factor of 4 for clarity.
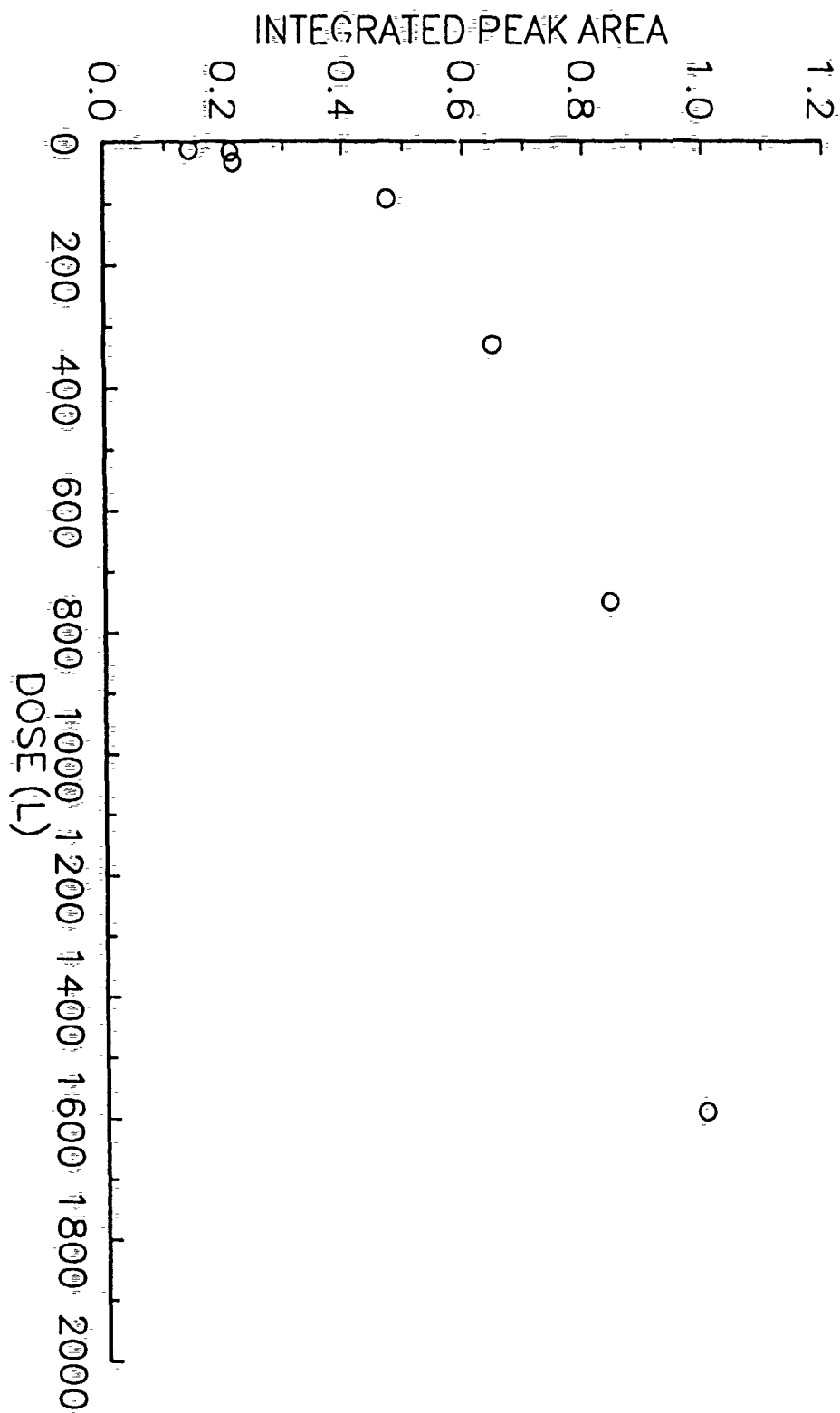
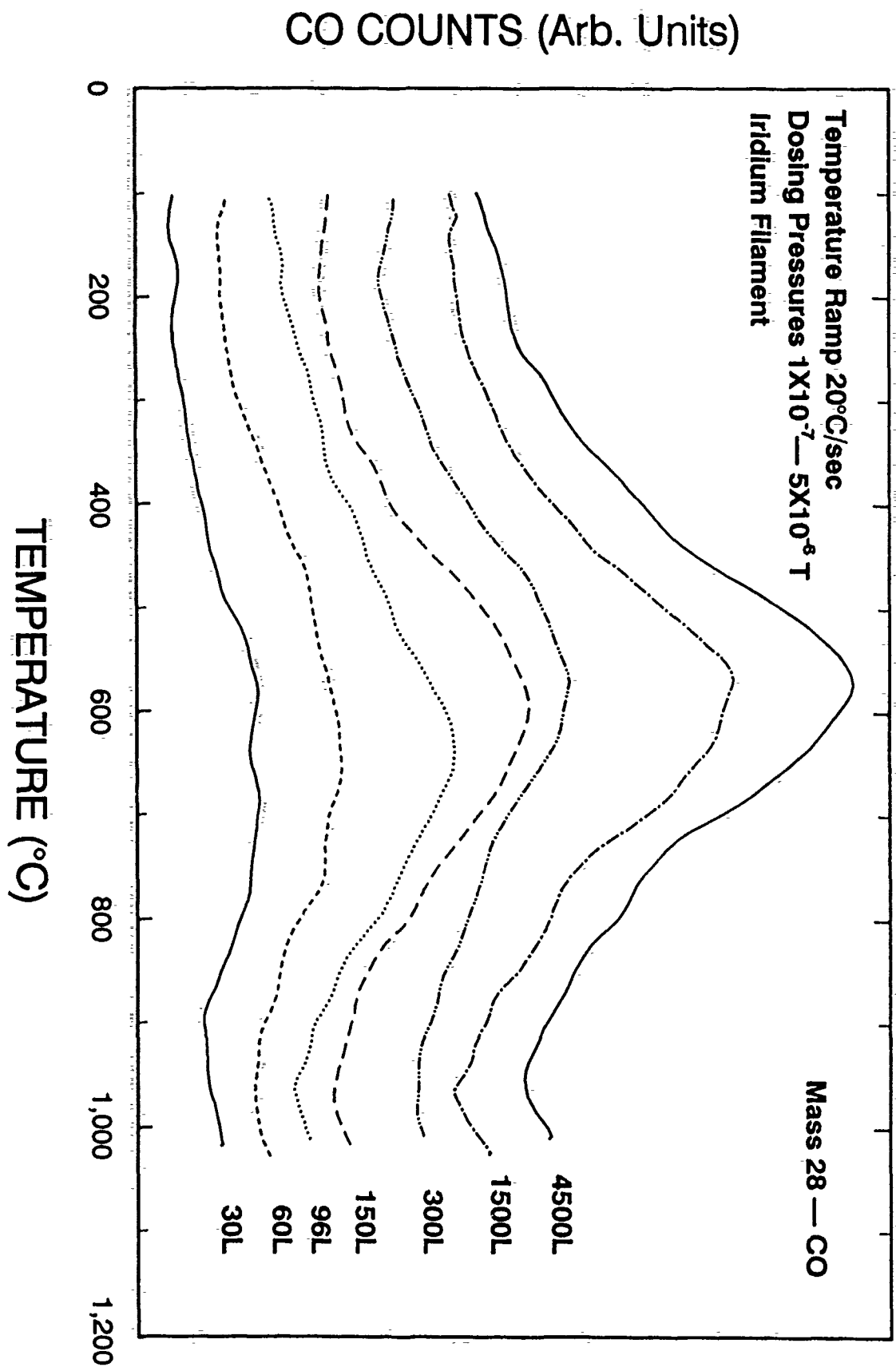Figure 7. Figure 7a shows a clean diamond (100) surface in the 2x1

configuration. Figures 7b and 7c show 2 possible oxygen bonding configurations which would give a 1x1 LEED pattern.
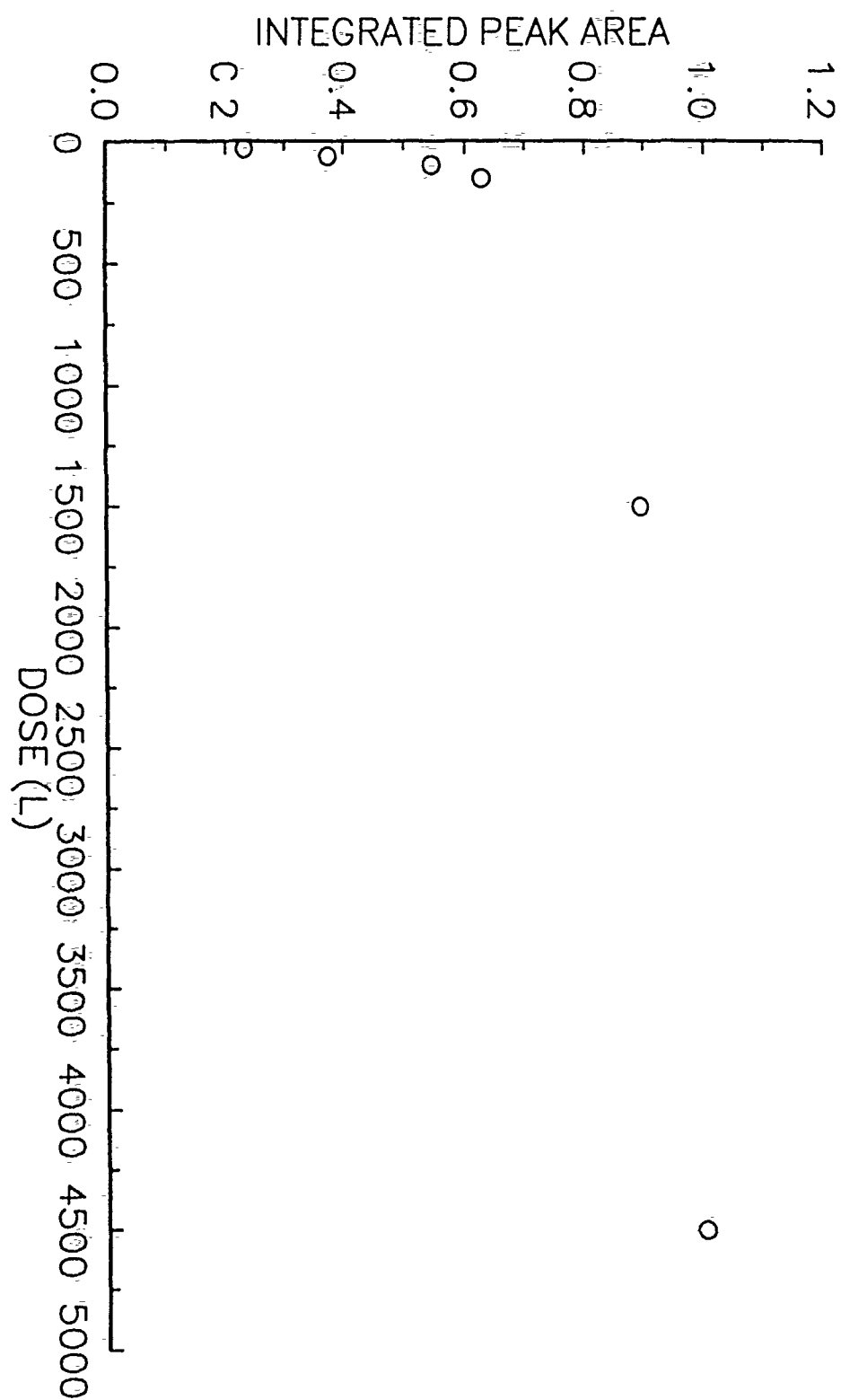
Substrate Mounting

Cr/Al
Thermocouple

.010" Moly Foil

.005" Moly Tabs

8 " Viewport

Hot Ni Tube
(Atomic Fluorine Source)

In Vacuo
Transfer

Stainless Steel cap
with 2mm aperture
to isolate Mass
Spectrometer

Manipulator for
direct resistive
heating of fixed
samples

LEED/Auger

To
MBE
&
ECOSS

Quadropole
Mass
Spectrometer
Differentially
Pumped with 1000
L/sec Turbopump
&
H2 Getter Pump

Gas
Dosing Port
(Iridium Filament
Atomic Oxygen
Source)

Kaufman
Source
Differentially
Pumped with 8"
Cryopump

Gas Dosing Port
(Tungsten Filament
Atomic Hydrogen
Source)

To
H
Cleaning
Reactor
&
CVD
Reactor

24

HYDROGEN COUNTS (Arb. Units)

2X1 : H Surface
Temperature Ramp 20°C/sec
Dosing Pressures 7X10⁻⁸ — 5X10⁻⁶ T

TEMPERATURE (°C)

1590L
750L
330L
93L
33L
16L
12L

200   400   600   800   1,000   1,200

CO COUNTS (Arb. Units)

Temperature Ramp 20°C/sec
Dosing Pressures 1X10⁻⁷—5X10⁻⁶ T
Iridium Filament

Mass 28 — CO

4500L
1500L
300L
150L
96L
60L
30L

TEMPERATURE (°C)

0   200   400   600   800   1,000   1,200

COUNTS (Arb. Units)

TEMPERATURE (°C)

Temperature Ramp 20°C/sec
O / O_2 Dose 300 sec — $5X10^{-8}$ T

Mass 28 — CO

Mass 44 — CO_2
X4

29

a)

Bare Diamond (100) 2 x 1 Structure

b)

Diamond (100) 1 x 1:O Bridging Structure

c)

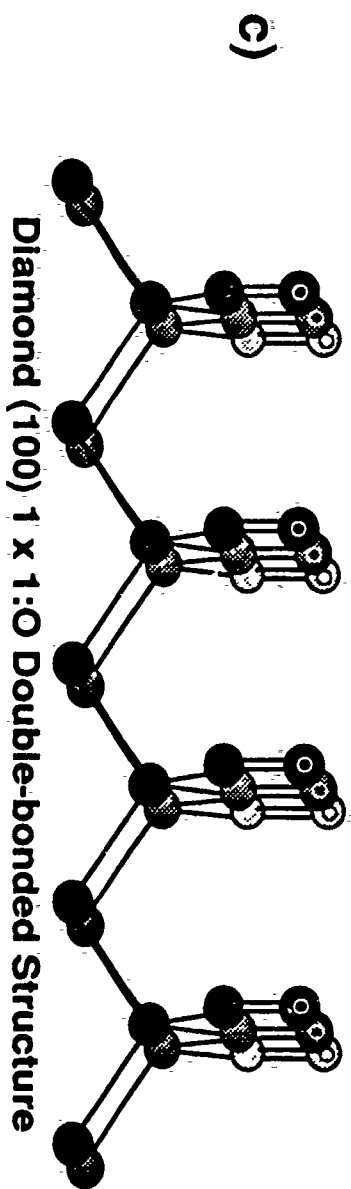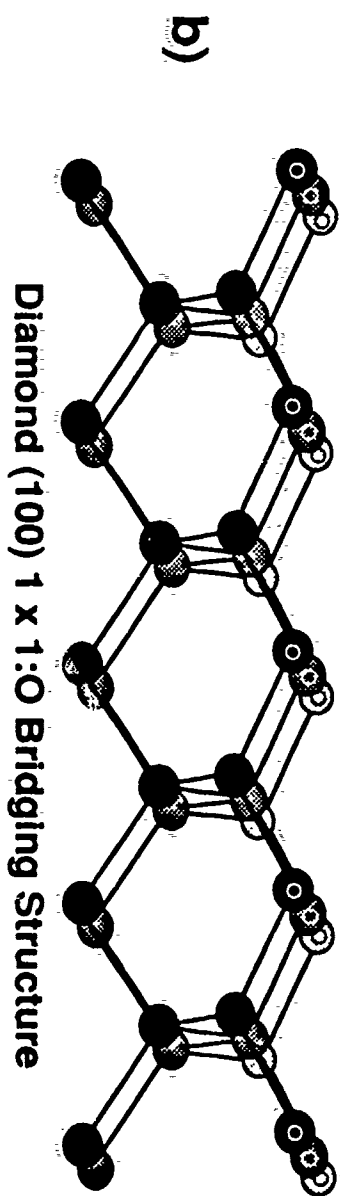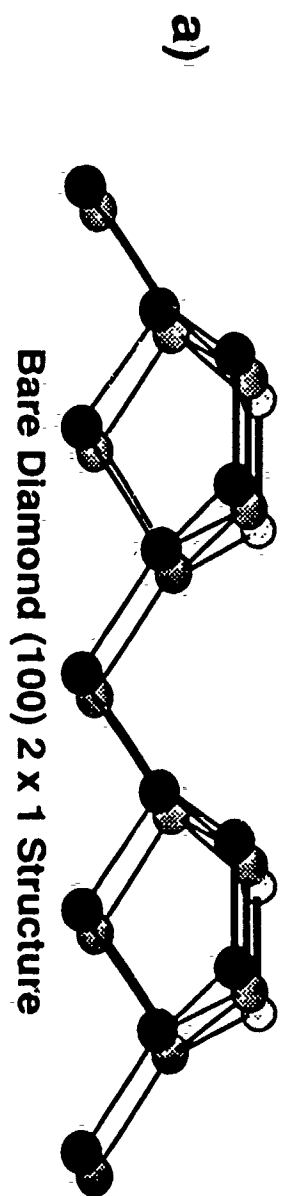**Diamond (100) 1 x 1:O Double-bonded Structure**

30

3.0 WATER-BASED DIAMOND GROWTH

To date, diamond films produced by chemical vapor deposition techniques have been grown principally heavy dilution of organic gasses with molecular hydrogen. The role of molecular hydrogen to the process is manifold, but the dissociation of molecular hydrogen into a high fraction of atomic hydrogen is critical to diamond stabilization and growth. A plethora of techniques have been applied to create concentrations of atomic hydrogen sufficient for high quality diamond growth. Typically, these techniques involve a high-temperature region (hot-filament, oxy-acetylene torch, microwave plasma, dc arc discharge, etc.) wherein high dissociations of molecular hydrogen is feasible. A low pressure rf-inductive plasma-assisted chemical vapor deposition technique has been developed for the growth of diamond which does <u>not</u> require molecular hydrogen as a process gas. Rather, the atomic hydrogen necessary for diamond growth (in this process) is supplied from plasma-dissociation of water vapor. Alcohols are mixed with the water to provide a convenient carbon source for diamond growth. In addition to the water-alcohol vapors, it has been observed that addition of acetic acid to the CVD process enables diamond growth at reduced rf power levels and consequently at lower substrate temperatures.

A description of the chemical vapor deposition system used in this work has been previously reported. The system produces diamond from both traditional H_2 - CH_4 mixtures as well as the water:alcohol:organic-acid solutions. The system consists of a 50 mm id plasma tube appended to a standard six-way cross. A radio frequency (13.56 MHz) induction coil couples power from the rf power supply into the plasma discharge.

31

Samples are located on a graphite carrier located immediately underneath the induction plasma. The rf excitation induces currents in the graphite susceptor which serve to heat the sample. Samples are introduced into the vacuum system via a vacuum load-lock which isolates the main chamber. The gasses (water, alcohol, acetic-acid) are introduced into the chamber through a leak valve on a storage tank which contains solutions of the water/alcohol or water/acetic-acid/alcohol. Vapors above the liquid are pumped from the storage tank into the growth chamber. The vapor pressure of the constituents above the liquid should be a product of their molar concentration and their respective vapor pressures. Water and alcohol solutions at room temperature have sufficient vapor pressures to supply a low pressure discharge ($<$ 10 Torr). High pressure operations might require the liquid solutions to maintained at an elevated temperature. For the growths reported here, vapors from various volumetric mixtures have been evaluated for diamond growth. The leak rate into the growth chamber from the solutions results in a loss of $\sim$ 0.2 cc/min from the liquid solutions. While there will be some depletion of the higher vapor pressure component, the practice of mixing allows a convenient method for evaluating different ratios of water-to-alcohol without the necessity of a gas manifold.

Samples are introduced to the growth system through a vacuum load lock. Prior to insertion, samples have been subjected to a diamond abrasive treatment with 1 μm diamond paste to enhance nucleation. Diamond growth proceeds by initiating an rf induction plasma with sufficient power to magnetically couple to the gas. J. Amorrim et al. has shown that rf coils couple by E-field at low powers and by B-field coupling at

higher powers. The B-field coupling is characterized by an intense plasma luminescence from a region of high density electrons, $\sim 10^{12}$ cm^{-3}. The E-field coupling at lower powers results only in a low density plasma, $\sim 10^{10}$ cm^{-3} with weak plasma luminescence. Introduction of water vapor alone to a low pressure (1.0 Torr) rf inductive discharge results in intense atomic H emission. OH emission lines are clearly visible but not as dominant as the atomic H emission lines. One thus observes that water discharges are capable of generating ample atomic H. Diamond growth then proceeds by introducing alcohol vapors into the plasma discharge along with the water vapor.

A. Water:alcohol results

We have previously reported the growth of polycrystalline diamond films using water/methanol, water/ethanol, or water/isopropanol mixtures. In that work, the vapor mixture entered the deposition system and diffused from the main chamber into the plasma tube. The vapors were not admitted into the system through the plasma gas feed. For this work, the storage bottle containing the liquid solutions was located on the plasma gas feed. Various water-alcohol mixtures were used to determine the effect of the C/O ratio on diamond growth. Figure 1 shows SEM micrographs from samples deposited from volumetric water-methanol mixtures ranging from 80% methanol to 33% methanol. The results for 80% methanol produce poorly faceted diamond. These results contrast remarkably from the work by Buck et al. and Bachmann et al. in a microwave discharge at higher pressures using 100% methanol. In that work, high quality diamond was obtained from only methanol. In this work, water addition to the methanol is critical to the formation of well-faceted crystalline

diamond. As observed in Figure 1, the quality of diamond growth increases as the methanol volumetric concentration is reduced. At 33% methanol in the water solution, well-faceted diamond growth is observed. From the respective vapor pressures of water and methanol at 20°C, we estimate the vapor pressures of water and methanol to be 11.7 and 31.5 Torr, respectively, above the 33% methanol mixture. Using these vapor pressures, one calculates the C/C+O, the O/O+H, and the H/C+H ratios to be 0.42, 0.22, and 0.83, respectively. According to the deposition phase diagram of Bachmann, the low C/C+O ratio of 0.42 should result in no diamond growth. Nonetheless, this oxygen rich ratio is necessary for diamond growth in this system. As noted in the P.K. Bachmann work, actual gas phase concentrations may vary due to interactions of the plasma with the carbonasceous walls of the reactor or in this case a graphite susceptor.

At high methanol concentration, diamond bonding as evidenced by a distinct feature at 1332 cm^{-1} s was not observed. Besides an amorphous carbon feature broadly centered at 1500 cm^{-1}, the Raman spectra also show a prominent feature near 1140 cm^{-1}. Nemanich et al. have observed this feature previously in film deposited with high CH$_4$ concentrations in microwave discharges. The addition of more water vapor to the process (analagous to the addition of more H$_2$ to the H$_2$/CH$_4$ microwave process) produces films with distinctive 1332 cm^{-1} Raman scattering. The film deposited a liquid solution of 33% methanol in water shows a distinctive 1332 cm^{-1} Raman scatter as well as some amorphous carbon component at 1500 cm^{-1} in the Raman spectrum.

B. Acetic-acid:water:methanol results

It was observed that diamond growth from the water-alcohol solutions required less rf power than diamond growth from more traditional H_2/CH_4. The lower rf power requirement is most likely a consequence of the lower ionization potentials of water and methanol. A list of ionization potentials is given below. The lower ionization potentials permit lower rf power levels to be applied for sufficient plasma ionization. Correspondingly, addition of organic acids to the water solutions substantially reduces the critical power necessary to magnetically couple. At present, we believe this observation is a consequence of a low ionization potential for the acetic acid molecule.

As a consequence, diamond growth in the low-pressure rf-induction plasma can be evaluated at lower substrate temperatures (through reduction in the induced current in the graphite sample carrier). Figure 2 shows SEM micrographs of diamond films deposited using 2:2:1 acetic-acid:water:methanol. The sample temperature is reduced from one sample to the next by the reduction in rf applied power. The growths at all temperatures show well-faceted diamond polyhedra. There appears to be no severe degradation of the film properties despite the $\sim 300\,^\circ$C reduction in growth temperature. Indeed, Raman spectra shown in Figure 3 from these samples would seem to indicate that higher quality growth was achieved between 300-400$\,^\circ$C than at the higher temperatures. All these films showed an amorphous carbon component at 1500 cm^{-1}. The reduction in applied power did reduce the deposition rate. The film deposited at 575$\,^\circ$C grew at a linear rate of 6000 Å/hr while the film deposited at 300 C grew at a linear rate of 2000 Å/hr.

The growth of diamond is undoubtedly facilitated in the low-pressure rf-induction plasma by the high electron density achieved when at a critical power the coupling changes from E-field to B-field coupling. In this work, we have replaced molecular hydrogen and methane with various mixtures of water, alcohols, and organic acids. The vapor discharges from the water-based solutions are easily ionized in the rf plasma owing to lower ionization potentially for the water, alcohol, and acetic acid molecules as compared to H_2 and CH_4. As a consequence, lower power levels are necessary for a B-field coupling.

Once the B-field coupling occurs, the high electron density and high electron temperature allows atomization of the parent molecules. Atoms and free radicals of both graphite etchant species such as H and OH and carbon-containing radicals are present at the diamond growth surface. Dissociation of those species will depend directly on the bond strengths. If one compares the bond-strengths for the various molecules and radicals used here, a number of interesting observations are apparent. A table of bond strengths is given below. First, the H-OH bond is not significantly weaker than the H-H bond. Thus, the high generation of atomic hydrogen from water discharges is probably a consequence of the lower ionization potential (allowing B-field coupling to be achieved at lower input rf powers) and a a consequence of the larger cross-section for electron-impact dissociation. Second, the bond strengths for H-liberation for a radical such as CH_2O-H from the methanol has a significantly lower dissociation energy than the parent CH_3O-H molecule. The CH_2O-H dissociation energy is also significantly lower than any of the energies for methane, methyl, or methylene dissociation. One

would expect that electron energies in the plasma sufficient to dissociate on a hydrogen from the methyl group on the alcohol would be more than sufficient to dissociate the CH_2O-H bond. And third, the lowest dissociation energies for H- liberation are found for the carboxyl radical COO-H. These radicals are contained on the organic acid and halogenated organic acid groups. It is the dissociation of this bond that gives acidity to water solutions containing these organic molecules. One would expect then that the organic acids would readily release H atoms to the plasma gas. The organic acid group behaves as graphite solvent in this process. To date, we have not been successful in depositing diamond from solutions of exclusively water and acetic acid. Concentrations of acetic acid in excess of 80% in water solution have not been evaluated. For the concentrations of acetic acid that we are using for the low temperature diamond growth 2:2:1 (acetic-acid:water:methanol), the primary roles of the organic acid group are (1) to promote ionization in the rf induction coil and (2) to contribute H atoms to the growth process.

We have previously been discussing mechanisms by which the water-based processes promote diamond growth in low-pressure rf-induction plasmas. These mechanisms have all been concerned with H- atom generation. At low pressures, diffusion of H atoms to walls and recombination of H atoms on the walls limit the steady-state population of H atoms. The steady state population being the difference of the generation and loss rates. The water-based processed (besides producing higher generation rates per unit power than the molecular-hydrogen based processes) may also significantly reduce the loss rates at low pressure. Water passivation of tube walls in

flowing afterglow hydrogen discharges has been used to reduce wall recombination. Water vapor (integral to the diamond growth in this work) would continuously passivate the reactor walls. Indeed, it might be possible to maintain the reactor walls at low a enough a temperature to condense multiple layers of water on the plasma tube walls. The water condensate would serve to buffer the wall materials from the extremely aggressive plasma environment. In addition to wall passivation, the water-based process may also reduce loss rates by permitting H^+ complexing with neutral H_2O water molecules. The hydronium ion H_3O^+ as in acidic-water solutions should rema' highly reactive, yet complexed so as to retard rapid diffusion to the plasma walls. It, thus 'eems plausible that the water-based processes for diamond growth can enhance diamond growth both by permitting higher generation rates of active species and by reducing loss mechanisms.

A low pressure chemical vapor deposition technique using water-alcohol vapors has been developed for the deposition of polycrystalline diamond films and homoepitaxial diamond films. The technique uses a low pressure (0.50 - 1.00 Torr) rf-induction plasma to effectively dissociate the water vapor into atomic hydrogen and OH. Alcohol vapors admitted into the chamber with the water vapor provide the carbon balance to produce diamond growth. Unlike previous results obtained from microwave sources using only methanol or Ar/methanol mixtures, the rf-induction source grows poor quality diamond unless water vapor is admitted. At 1.00 Torr, high quality diamond growth occurs with a gas phase concentration of water approximately equal to 47% for methanol, 66% for ethanol, and 83% for isopropanol. In the operation of the rf induc-

tion plasma, there exists a critical power level at which the coupling to the plasma changes from E-field coupling to B-field coupling. The B-field coupling has been shown in Ar plasmas to produce about two orders of magnitude increase in the electron density.[1] We have observed that the critical power to achieve B-field coupling is substantially lower for the water-based processes as compared to the traditional molecular hydrogen-based processes. Furthermore, reduction in the critical power necessary to B-field couple is achieved through the addition of acetic acid to the water:alcohol solution. The water-alcohol vapors permit diamond growth to occur at lower power levels as compared to the H_2/CH_4 discharges. The lower input power level required in turn reduces substrate-carrier inductive heating and allows lower temperature diamond growth. Currently, diamond depositions using water:methanol:acetic-acid are occurring as low as 300°C with only about 500 W power input to the 50 mm diameter plasma tube.

Low Temperature Diamond Growth
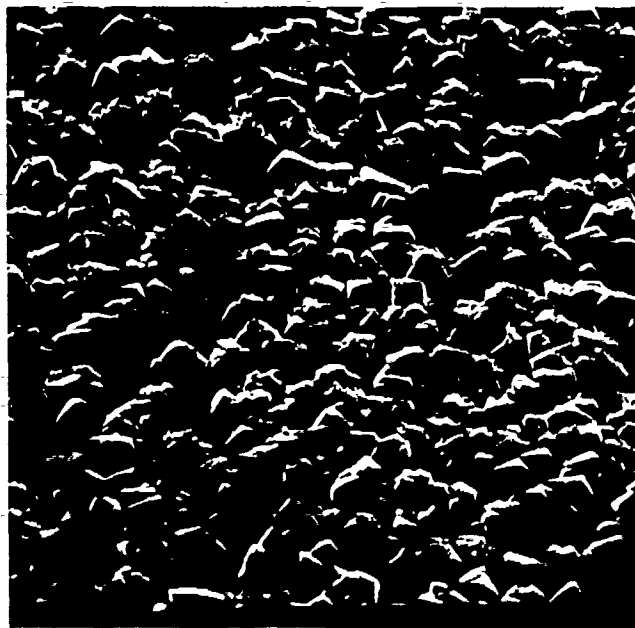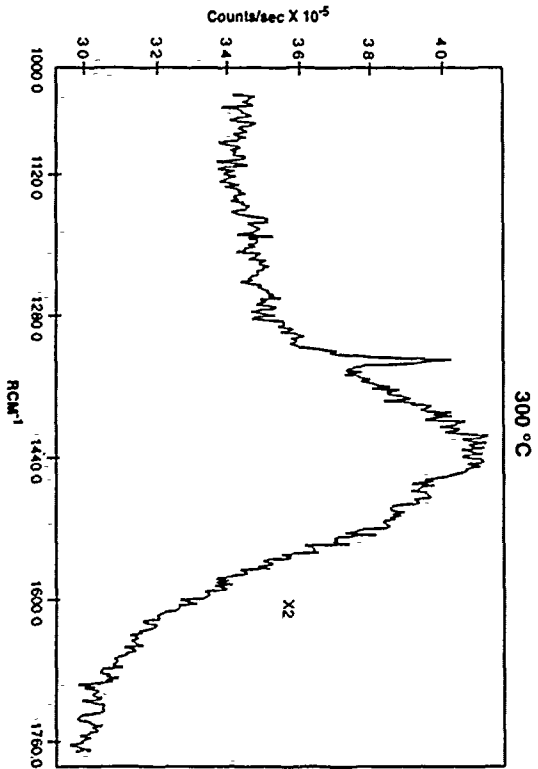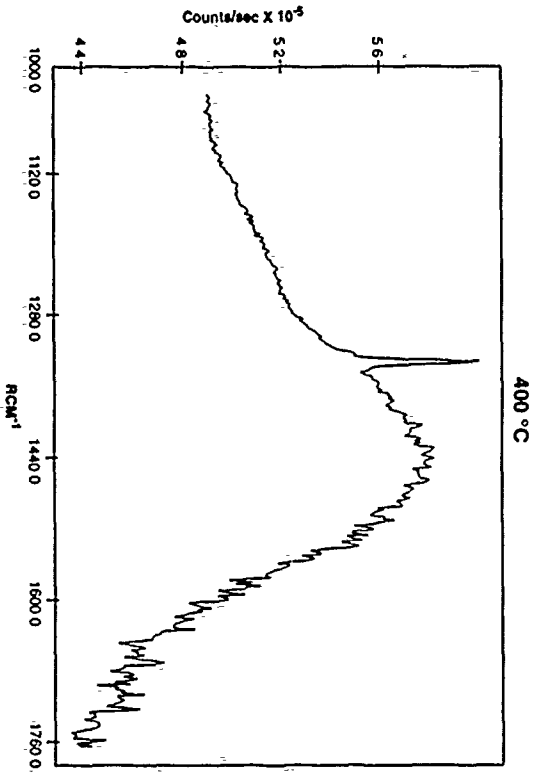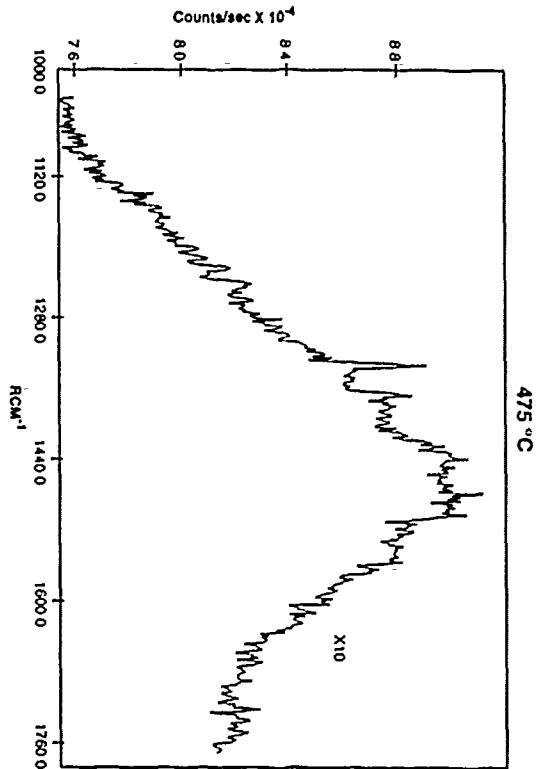
550 °C
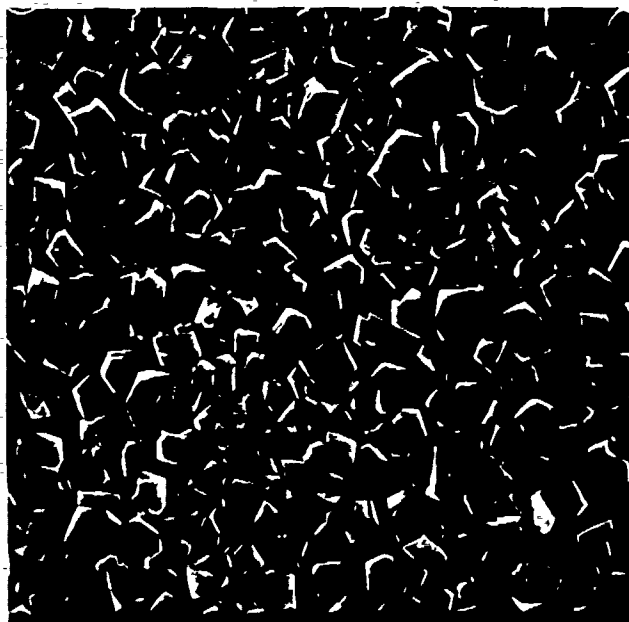
5.0 µm

475 °C

5.0 µm

400 °C

5.0 µm

300 °C

5.0 µm

RTI

Low Temperature Diamond Growth

550 °C

400 °C

475 °C

300 °C

41
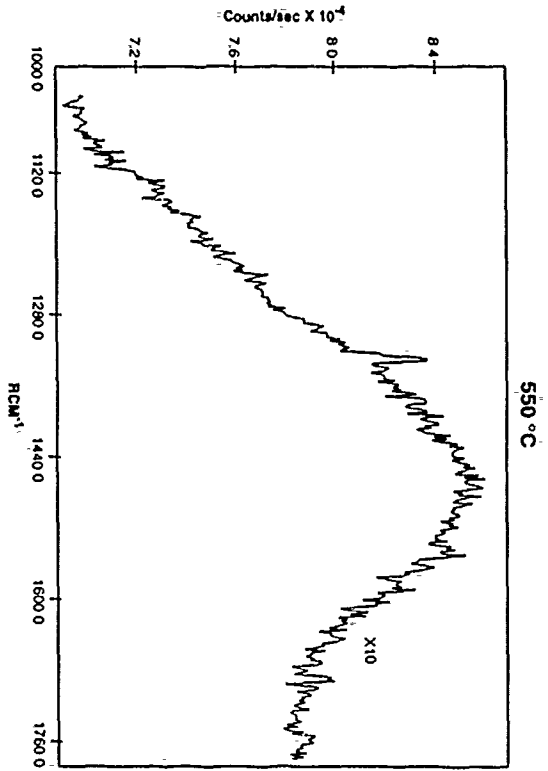
IONIZATION POTENTIALS

Table D.1 Ionization potentials of some molecules and radicals[†]

Molecule or radical	IP, eV	Molecule or radical	IP, eV	Molecule or radical	IP, eV
H_2	15.43	CO	14.01	HS	10.41
BH	9.77	CO_2	13.77	H_2S	10.47
BH_2	~9.8	NO	9.26	CS[*]	~11.33
BH_3	~12.3	N_2O	12.89	NS	~9.85
B_2H_6	11.39	NO_2	9.75	SO	10.34
CH	10.64	CH_3OH	10.84	SO_2	12.33
CH_2	10.40	F_2	15.69	SO_3	~11.0
CH_3	9.84	HF	16.01	S_2O	~10.3
CH_4	≤12.62	BF_3	15.56	SF_4	12.28
C_2H_2	11.41	CF_3	9.17	SF_6	15.35
C_2H_4	10.51	NF_3	13.00	Cl_2	11.49
C_2H_6	11.52	SiH_4	11.66	HCl	12.74
C_6H_6	9.25	Si_2H_6	~10.2	BCl_3	11.62
N_2	15.58	P_4[‡]	9.2	GeH_4	11.31
NH_3	10.16	PH_3	9.98	Ge_2H_6	~12.5
CN	14.1	PF_3[§]	11.66	AsH_3	10.04
HCN	13.59	OPF_3	12.75	H_2Se	9.88
CH_3NH_2	8.97	CH_3PH_2[§]	9.12	Br_2	10.51
$(CH_3)_2NH$	8.24	$(CH_3)_2PH$[§]	8.47	HBr	11.67
$(CH_3)_3N$	7.81	$(CH_3)_3P$[§]	8.11	SbH_3	9.58
C_5H_5N	9.27	$P(OCH_3)_3$[§]	8.50	H_2Te	9.14
O_2	12.07	S_2	9.36	I_2	9.39
H_2O	12.61	S_8	9.04	HI	10.39

† Except as noted. data are from H. M. Rosenstock, K. Drexl, B. W. Steiner, and J. T. Herron, *J. Phys. Chem. Ref. Data*, **6**, suppl. 1 (1977). See Table 1.7 for atomic ionization potentials.

‡ C. R. Brundle, N. A. Kuebler, M. B. Robin, and H. Basch, *Inorg. Chem.*, **11**, 20 (1972).

§ R. V. Hodges, F. A. Houle, J. L. Beauchamp, R. A. Montag, and J. G. Verkade, *J. Am. Chem. Soc.*, **102**, 932 (1980).

* N. Jonathan, A. Morris, M. Okuda, K. J. Ross, and D. J. Smith, *Faraday Discuss. Chem. Soc.*, **54**, 48 (1972).
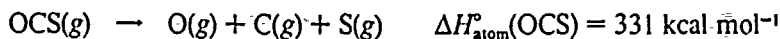
Table 3.9 Dissociation energies of some gaseous diatomic molecules at 298 K

Molecule	D, kcal mol^{-1}	Molecule	D, kcal mol^{-1}
H_2	104.2	LiCl	114
D_2	106.0	BeCl	93
		BCl	128
HF	135.8	CCl	80
HCl	103.2	OCl	64.3
HBr	87.5	NaCl	98
HI	71.3	MgCl	74
LiH	58	AlCl	118.1
BH	79	KCl	101.5
CH	81	CuCl	78
NH	75	AgCl	75
OH	102.3	HgCl	25
NaH	48		
AlH	68	O_2	119.1
PH	73	S_2	102.6
SH	85	SO	124.7
KH	44	Se_2	73.6
HgH	10	Te_2	53.8
F_2	37.8	BeO	107
Cl_2	58.2	BO	182
Br_2	46.1	CO	256.9
I_2	36.1	NO	151.0
		MgO	91
ClF	61.0	AlO	116
BrF	59.4	SiO	190
IF	66.2	PO	141
BrCl	51.5	BrO	56.3
ICl	49.6		
IBr	41.9	C_2	142.4
		Si_2	81
LiF	137	Pb_2	13
BeF	147		
BF	180	N_2	226.0
CF	129	P_2	117
NF	72	Sb_2	70
OF	52	PN	168
NaF	115		
MgF	107.3	Li_2	26
AlF	159	Na_2	18
KF	118.1	K_2	13
		Cu_2	46
		Ag_2	37
		CN	183
		CS	183
		B_2	71

Table 3.10 Some bond dissociation energies of gaseous molecules and radicals

Molecule	D, kcal mol^{-1}	Molecule	D, kcal mol^{-1}
HO—H	119	CH_2=NH	154
CH_3COO—H	112	H_2N—NH_2	58
H_3CO—H	102	HO—OH	51
HOO—H	90	NH_2—Cl	60
C_6H_5O—H	85	HO—Cl	60
ClO—H	78	HO—I	56
NC—H	130	OO—H	47
Cl_3C—H	96	CH_2O—H	31
HC≡CH	230	COO—H	12
HC≡N	224	CH_2—H	106
CH_2=CH_2	163	CH—H	106
CH_2=O	175	CH_2CH_2—H	39
HN=O	115		

the molecular fragments that form when a bond in a molecule is broken. Unfortunately, the sum of the separate dissociation energies of the bonds of a molecule is not equal to the energy of dissociating the molecule completely into atoms. For example, consider the molecule OCS:

$$OCS(g) \longrightarrow CO(g) + S(g) \qquad D(OC{=}S) = 74 \text{ kcal mol}^{-1}$$

$$OCS(g) \longrightarrow O(g) + CS(g) \qquad D(O{=}CS) = 31 \text{ kcal mol}^{-1}$$

$$OCS(g) \longrightarrow O(g) + C(g) + S(g) \qquad \Delta H^\circ_{atom}(OCS) = 331 \text{ kcal mol}^{-1}$$

The sum of $D(OC{=}S)$ and $D(O{=}CS)$ is much less than the atomization energy of OCS. However, each of the sums $D(OC{=}S) + D(C{\equiv}O)$ and $D(O{=}CS) + D(C{\equiv}S)$ must equal the atomization energy of OCS.

At least a few remarks should be made regarding the methods used to obtain dissociation energies. In most cases, the dissociation energies were calculated from heats of formation such as those given in Appendix E and Table 3.12. Thus from the heats of formation of HCl(g), H(g), and Cl(g), one can readily calculate D(H—Cl). The heat of formation of HCl(g) was obtained by directly measuring the heat of reaction of H_2 and Cl_2 in a calorimeter; the heats of formation of H(g) and Cl(g) are calculated from the dissociation energies of H_2 and Cl_2, which in turn were obtained from electronic absorption spectral data. The heats of formation of molecules such as NaCl(g), which at room temperature are unstable with respect to crystalline phases, obviously cannot be directly measured in a calorimeter. One method for obtaining the heat of formation of such gaseous molecules is by measuring the vapor pressure of the diatomic molecule over the solid as a function of temperature. From the derived heat of vaporization and the known heat of formation of the solid (obtained calorimetrically), one readily

High-density plasma mode of an inductively coupled radio frequency discharge

J. Amorim, H. S. Maciel, and J. P. Sudano

Departamento de Física-ITA/CTA, 12225, São José dos Campos, SP, Brazil

Experimental observations concerning the formation of a high-density plasma in an inductively coupled radio-frequency (11.4 MHz) discharge in argon are described. These observations are complemented by probe measurements that provide a quantitative description of plasma properties over an useful range of vapor pressure, 0.02–0.2 Torr, and rf power, 50–400 W. It is shown that a dense plasma of the order of 10^{12} cm^{-3} can be easily formed, having the configuration of a luminous plasmoid embedded in a low-density, 10^{10} cm^{-3}, diffuse plasma.

I. INTRODUCTION

The early works on the origin of an inductively coupled radio frequency (rf) discharge were carried out at the beginning of this century.[1-3] These works lead to the conclusion that at low excitation the discharge is of electrostatic origin (E discharge) and at high excitation it is of electromagnetic origin (H discharge).[4] The E discharge is characterized by a faint glow that extends throughout the discharge tube. By increasing the rf power, a transition to the H discharge may occur, which is characterized by the appearance of a localized plasma formation having the aspect of a luminous body embedded in a faint plasma that still remains from the E discharge. The rf discharges between parallel electrodes exhibit similar features regarding the visible aspect of the discharge, i.e, the conventional diffuse glow and, under certain conditions, the formation of a luminous plasma surrounded by a diffuse glow. The word "plasmoid" was coined to identify these luminous bodies.[5] Extensive investigations[6,7] have been made towards the better understanding of these phenomena. However, the physical mechanism of plasmoid formation in rf discharges is by no means clear.

Quantitative data have shown that in the regime in which the plasmoid is formed the plasma density can attain typical values of the order of 10^9 cm^{-3} in capacitively coupled rf discharges[6,7] and 10^{12} cm^{-3} in inductively coupled rf discharges.[8]

In the present work an experimental investigation concerning the plasma properties in an inductively coupled rf (11.4 MHz) discharge of the type known as barrel reactor is reported. This kind of reactor is widely used for plasma polymerization. First both the low-density plasma mode (E mode) and the high-density plasma mode (H mode) of the discharge, are identified. Probe techniques are used to determine the profiles of the electron temperature and plasma density through the discharge volume, with a main objective of characterizing the high-density plasma mode of the discharge. The results show that a simple manner of obtaining a high-density plasma is by driving an inductively coupled rf discharge towards a plasmoid formation. This high-density plasma has already found application in a high rate sputtering apparatus described by Yamashita.[8]

II. EXPERIMENTAL SETUP

The diagram of the apparatus is shown in Fig. 1. The discharge tube is made of Pyrex, 25 cm long and 3.8 cm internal diameter. A seven-turn coil (helical antenna) made of 5 mm diameter copper tubing surrounds the tube and it is coupled to the rf power supply via a matching network. The rf power is measured at the output of the rf generator when optimum matching conditions (zero reflected power) are achieved. The residual pressure is about 10^{-6} Torr (1.3×10^{-4} Pa) and the discharge is made in argon at pressures in the range of 0.02–0.2 Torr. The rf power is varied from 50 to 400 W.

III. PROBE TECHNIQUE

In order to determine the plasma properties, single and double electrostatic probes were used. The effects of rf on probe measurements can be quite considerable since the amplitude exceeds the equivalent thermal potential, KT_e/e, of the plasma.[9] In order to minimize this effect, a choke is inserted in the probe circuitry, Fig. 2, the impedance of which is made much larger than that of the probe sheath. This technique, developed by Gagné and Cantin[10] is adopted in the present work to both kinds of probes. From the current-voltage characteristic of the probe and following the usual technique, we obtain the electron temperature T_e and the
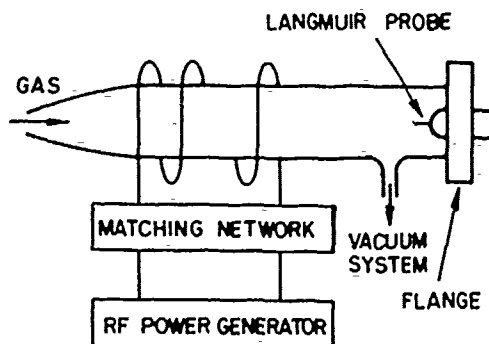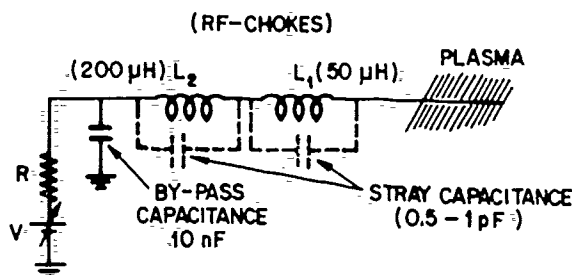

FIG. 1. Experimental apparatus.

FIG. 2. Diagram of the probe circuitry.

FIG 3 Axial density profile of the plasma in the E discharge.

plasma potential. The plasma density is obtained from the ion saturation region of the characteristic by using Laframboise's graphs. When there is no convenient reference electrode, or if the plasma is inhomogenous, then the double probe can be used. This system, as a whole, is floating and it is not possible to determine the plasma potential. The plasma density and electron temperature can be derived from the double floating-probe characteristic. The electron temperature, was derived by using the equivalent resistance method.[12]

$$T_e = e \sum I / 4KS, \tag{1}$$

where $\sum I$ is the total current drawn by the probe between the two saturation regions and S is the slope of the double-probe characteristic evaluated at $V = 0$. Peterson and Talbot[13] modified Eq. (1) so that it could be applied to the orbital-motion-limited (OML) region. The modified equation is

$$T_e = e \sum I(1 + \varepsilon)/4KS, \tag{2}$$

where ε is a function of the probe radius (r_p) and the Debye length (λ_D). The plasma density is calculated from the electron temperature and ion saturation current drawn by the probe, at a calculated normalized potential. Laframboise's graphs are applied to the OML regions in the range $r_p/\lambda_D \geq 1$. In the range $r_p/\lambda_D < 1$, the density obtained from this method is overestimated.[14]

IV. EXPERIMENTAL OBSERVATIONS AND RESULTS

The rf voltage applied to the coil was gradually increased until the occurrence of the gas breakdown and the development of a discharge of uniform glow along the whole tube. This is the E discharge. By increasing the rf power, a point is reached at which an abrupt change of the discharge properties are observed: the discharge changes suddenly into a well-localized plasma formation having the aspect of a luminous body concentrated in the inner region of the coil. This region is so bright that the glow formerly extending throughout the tube is not noticeable. We have then the H discharge. A moveable cylindrical probe was used to determine the plasma properties along the axis of the E-discharge. The metallic flange that touches the plasma is taken as a reference for the probe voltage. Typical electron temperatures are around 4 eV but decrease as the pressure is increased. The axial profile
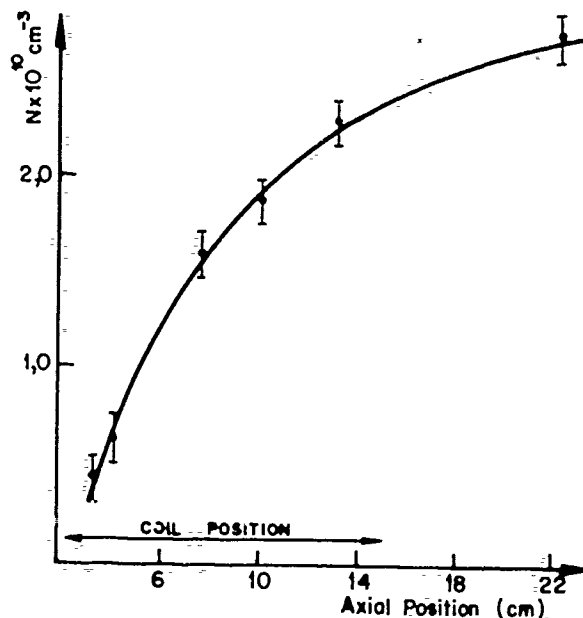
of the plasma potential is a straight line indicating a uniform electrical field of the plasma like in the case of a positive column of a dc discharge. The axial density profile of the E discharge is shown in Fig. 3.

The E discharge can be useful in plasma polymerization. As the polymer deposition rate depends on electron density,[15] the best region to place the substrate is upstream from the coil region, where the plasma density tends to be saturated.

In order to determine the properties of the H discharge, the use of a double probe is imperative because, in this case, the discharge is concentrated into a plasmoid which does not touch any convenient reference electrode. Figure 4 shows the plots of the plasma density in the inner region of the coil (position of 7.5 cm) as the rf power is increased from 50 to 400 W, and for two values of argon pressure.

The striking feature of these curves is the abrupt increase in the plasma density (two orders of magnitude) as the discharge shifts from the electrostatic to the electromagnetic mode. The electron temperature in the plasmoid is typically about 10 eV. At a pressure of 30 mTorr or lower the transition from E to H discharge occurs smoothly while at higher pressures it occurs suddenly.

By moving the double probe along the axis of the tube we determined the axial profiles of the electron temperature and electron density as shown in Figs. 5 and 6, respectively. There is an abrupt decrease of N and Te as the probe moves out of the plasmoid region. Another moveable double probe was used to determine the radial variation of T_e and N. Figures 7 and 8 indicate that, at the axis, the electron density and temperature are lower than at the bulk of the plasmoid.

A comprehensive view about the formation of E discharge and H discharge is provided by the work of Mackinnon.[3]
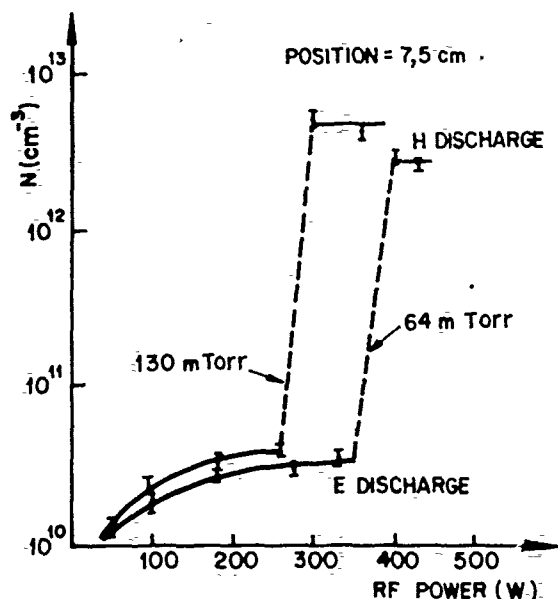
FIG. 4. Variation of the plasma density with rf power and the transition from E to H mode of the discharge.
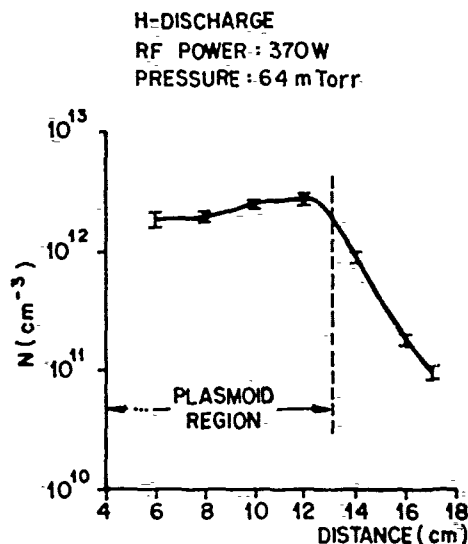

FIG. 6. Axial profile of the plasma density in the H discharge.

"At low excitation, the discharge is produced by electrostatic field (E_s) between the ends of the solenoidal coil. This field was shown by Townsend and Donaldson,[2,3] and confirmed by us, to be more than thirty times the field due to the eletromagnetic induction (E_m) around a ring inside the coil. For certain low excitation, the value of E_m is almost negligible, but that of E_s must be sufficient after subtracting the potential drop through the glass walls, to cause weak ionization in the gas. This gives rise to the faint electrostatic glow one gets in the E discharge. As the excitation is increased, the current tends to increase through the electrostatic path leading to an increase in ionization of the gas, and thus a lowering of its effective resistance to the electrostatic voltage. Hence,

although the total electrostatic voltage across the circuit is higher, the proportion of the voltage used up in the gas is less because the resistance of it has dropped whilst the resistance of the glass has remained the same. Thus, even though E_s increases externally, it does not do so at the same rate internally. On the other hand, E_m increases directly with the excitation. When ionization starts, the ring resistance drops but since the whole electromotive force is always applied to the ring circuit, the current in the path must increase more quickly than E_m. Thus intense ionization sets in around the ring when E_m attains a certain value."
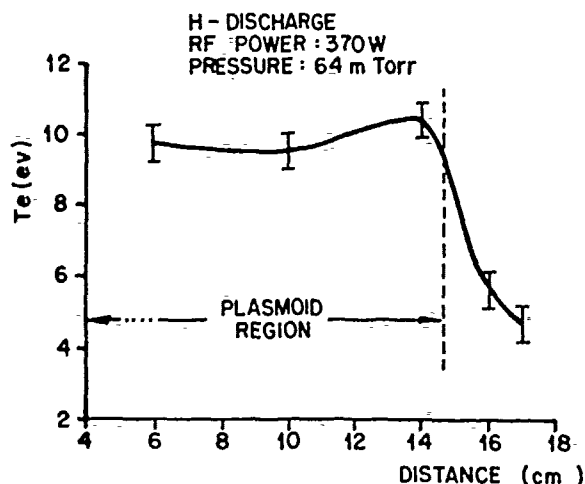

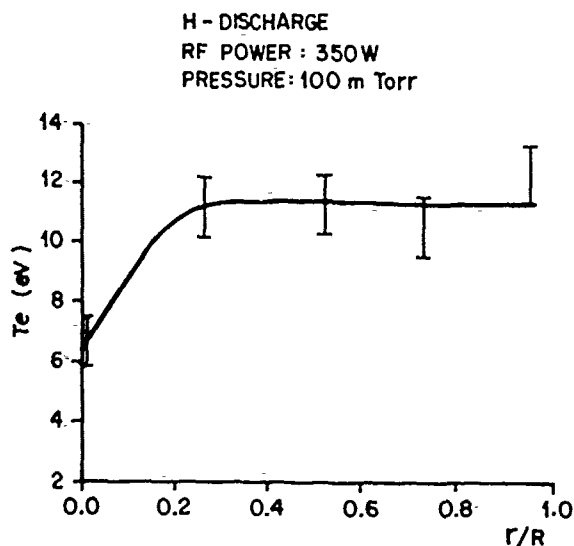FIG. 5. Axial profile of the electron temperature in the H discharge.

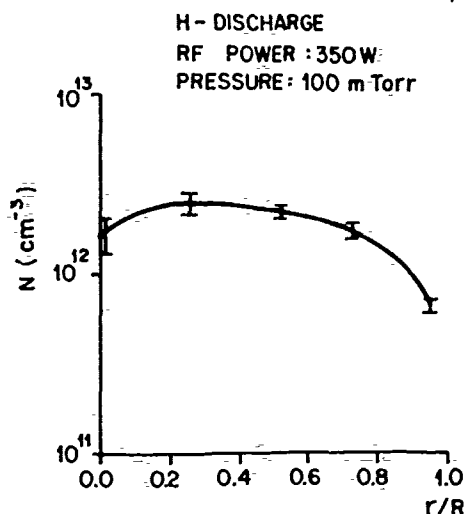FIG. 7. Radial variation of the electron temperature in H discharge

H – DISCHARGE
RF POWER : 350 W
PRESSURE : 100 m Torr

FIG. 8. Radial variation of the plasma density in the H discharge

FIG. 9. Schematic of the H discharge configuration and typical values of electron temperature and electron density.

The final configuration is that of high-density plasma, i.e., a plasmoid, embedded in a low-density plasma, as schematically shown in Fig. 9. Measurements of plasma potential have indicated a potential drop of ~ 10 V through the plasmoid border. This potential drop occurs in a double layer that separates the two plasmas.

The dense plasma formed in the sputtering apparatus described by Yamashita[8] are certainly originated from the H mode of the discharge. The explanation proposed by the author is rather consistent with the generation mechanisms of plasmoids in capacitively coupled rf discharges.[6]

V. CONCLUSIONS

We have reported experimental evidences of two modes of operation of an inductively coupled rf discharge: The E discharge in which a faint plasma is formed and the H discharge in which a high-density plasma is produced. The high-density plasma is characterized by measurements of the axial
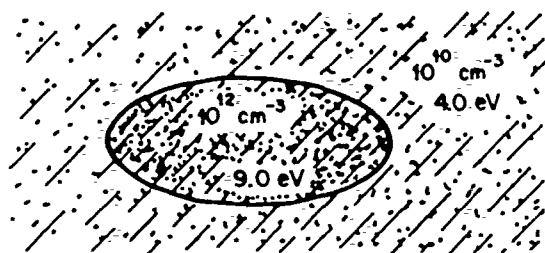
and radial profiles of electron temperature and plasma density.

In the steady state the dense plasma has a configuration of an ellipsoidal plasmoid but, in the present case, it has a much higher plasma density than the well known plasmoids formed in capacitively coupled rf discharge. In our case the generation mechanism of this strong plasmoid is related to the induction electric field while the capacitive coupled rf plasmoids are more likely to be related to the quasistatic rf field.[46] In both cases the plasmoid appears embedded in a diffuse glow of lower plasma density and the two plasmas are separated by a double layer.

[1] J. J. Thomson, Philos. Mag. 4, 1128 (1927).
[2] J. S. Townsend and R. R. Donaldson, Philos. Mag. 5, 178 (1928).
[3] R. W. Wood, Philos. Mag. 8, 206 (1929).
[4] K. A. Mackinnon, Philos. Mag. 8, 605 (1929).
[5] R. W. Wood, Phys. Rev. 35, 673 (1930).
[6] J. Taillet, Am. J. Phys. 37, 423 (1969).
[7] M. Sanduloviciu, Plasma Phys. 29, 1687 (1987).
[8] M. Yamashita, J. Vac. Technol. A 7, 151 (1989).
[9] V. A. Godyak and O. A. Popov, Sov. Phys. Tech. Phys. 22 (1977).
[10] R. R. J. Gagné and A. Cantin, Appl. Phys. 43, 6 (1972)
[11] R. M. Clements, J. Vac. Sci. Technol. 15, 193 (1978).
[12] E. O. Johnson and L. Malter, Phys. Rev. 80, 58 (1960).
[13] E. W. Peterson and L. Talbot, AIAA J. 8, 2215 (1970).
[14] M. G. Dunn and J. A. Lordi, AIAA J. 8, 1077 (1970).
[15] H. Yasuda, J. Polym. Sci. Macr. Rev. 16, 199 (1981).

Chemical vapor deposition of diamond films from water vapor rf-plasma discharges

R.A. Rudder, G.C. Hudson, J.B. Posthill, R.E. Thomas, R.C. Hendry, D.P. Malta, and R.J. Markunas, Research Triangle Institute, Research Triangle Park, North Carolina 27709-2194

T.P. Humphreys and R.J. Nemanich, North Carolina State University, Raleigh, North Carolina 27695-8202

Polycrystalline diamond films have been deposited from water vapor rf-plasma discharges at 1.0 Torr containing various alcohol vapors. No other gasses such as H_2, F_2, or Cl_2 were admitted to the growth chamber. Scanning electron microscopy and Raman spectroscopy have been used to characterize the diamond films. In addition, a water-ethanol mixture has been used for homoepitaxial deposition with a full-width-half-maximum narrower than the bulk substrate (2.60 cm^{-1} and 2.75 cm^{-1}, respectively). This technique represents a remarkable new approach to the growth of diamond which does not depend on delivery of hydrogen, fluorine, hydrocarbon, or halocarbon gasses that have been typically used by other workers. The nucleation density and topography of the polycrystalline diamond films deposited from the water alcohol mixtures are quite sensitive to the choice of alcohol. Water vapor discharges, by producing H atoms and OH radicals, become the functional equivalent to molecular H_2 discharges producing H atoms characteristic of many other diamond chemical vapor deposition techniques.

A variety of techniques have been developed for the deposition of diamond from the gas phase using plasma and thermal activation.[1-10] Early theories of diamond deposition hypothesized that the deposition of diamond was a codeposition process in which both diamond bonding units and graphitic bonding units were being deposited simultaneously.[1-2] Atomic hydrogen produced by dissociation of molecular hydrogen in plasma discharges, arc discharges, or hot filaments dissolves the non-diamond phases from the depositing layer and, thus, promotes the diamond phase. Recently, oxy-acetylene torches have been used to grow diamond films.[9-10] The oxy-acetylene flame, in addition to forming H_2O, CO, and CO_2 by-products, provides atomic hydrogen to the growth surface. Many gaseous carbon sources have been used for the deposition of diamond. Hydrocarbons, halocarbons, fluorocarbons, and alcohols have all been used in the deposition of diamond films. In a plasma or a thermally activated processes, those carbonaceous gasses are driven towards their high-temperature, equilibrium product distributions. Not surprisingly, the quality of the diamond films do not depend as critically on the carbon source as they depend on the C/H ratio or perhaps more appropiately the C/H/O ratio in the gas phase.[11] If one examines the list of radicals and gasses which gasify graphite, H atoms, F atoms, and F_2 molecules are included on the list.[12] Also present on the list are O atoms, OH radicals, and O_2 molecules. Oxygen has certainly been added to diamond producing environments, either by using carbon carriers containing oxygen or through intentional addition of oxygen to the gas stream in microwave discharges. Indeed, Buck et al.[13] have deposited diamond in a relatively limited set of conditions using only methanol or methanol/Ar mixtures. Initial microwave

plasma results showed an improvement in diamond growth with a small percentage of O_2 addition, but they also showed a degradation in crystalline quality for films deposited with more than 2% O_2 addition.[14] However, more recently the work of Bachmann et al.[11] and Chen et al.[15] has demonstrated that higher oxygen concentrations can certainly yield diamond deposition with correspondingly higher carbon concentrations.

We report here on a novel, low temperature growth technique for the chemical vapor deposition (CVD) of diamond films from low-pressure rf-plasma discharges containing principally water vapor. Carbon for diamond deposition was supplied to the plasma gas by admitting alcohol vapor with the water vapor. No other gasses were admitted to the growth chamber. Hence, this work is quite different from the work of Saito et al.[16,17] wherein 0- 6% concentrations of water in H_2 - CH_4 microwave plasmas were investigated for diamond growth. In this letter, predominantly water-based discharges produce OH and H radicals. The water discharge becomes functionally equivalent to hydrogen discharges in other diamond CVD techniques. Emission from a pure water discharge and the water-alcohol discharges described in this letter show strong H_α emission and OH emission. The atomic hydrogen emission from a pure water rf-plasam discharge at 1.0 Torr is so dominant that the plasma has a charcteristic red color from the 656 nm emission. The ratio of water to alcohol admitted to the growth chamber was fixed by the partial pressures of water and alcohol above the mixed solutions of 20% alcohol in water. The morphology of the polycrystalline films was dependent on the choice of alcohol. Distinct differences were observed both in nucleation

density and crystalline morphology. In addition to polycrystalline growth, homoepitax-ial diamond growth has been accomplished.

Study of polycrystalline diamond growth in the water vapor system was under-taken using Si(100) substrates. Prior to introduction into the growth chamber, the samples were subjected to polishing with graphite fibers[18] and/or diamond paste to promote nucleation. Descriptions of the growth system have been reported elsewhere.[19] The samples are located on a graphite susceptor just beneath a three-turn rf induction coil. The rf induction coil maintains the water vapor discharge and heats the graphite susceptor upon which the sample is located. The liquid mixture is stored in a metal flask connected to the vacuum chamber by a manual leak valve. Once the sample is in position and the chamber is evacuated, the water vapor/alcohol gas mixture is metered into the chamber at a rate of ~ 20 sccm. The vapor mixture was admitted into the chamber not through the plasma tube but rather was admitted into the metal vacuum cross at the base of the plasma tube. The ratio of water to alcohol admitted is deter-mined by the product of the mole fractions of water and alcohol in the liquid and the respective vapor pressures of the water and the selected alcohol. A process pressure control valve is used to vary the effective pumping speed in order to maintain a pres-sure in the growth chamber of 1 Torr. To initiate deposition, a 1000 W, 13.56 MHz signal is applied to the rf coil. The power level results in a sample temperature of 625 ° C during deposition. Following 2 hours of deposition, the samples were removed from the reactor and examined with the scanning electron microscope (SEM) prior to Raman analysis. Figure 1 shows electron micrographs of the samples deposited for 2

hours using water vapor mixtures containing either methanol, ethanol, or isopropanol. The micrographs show that the nucleation is highly dependent on the choice of alcohol. The alcohols with the higher vapor pressure nucleate at a higher density. If one uses the average crystallite size as a measure of the growth rate, the growth rate does not vary considerably with the choice of alcohol. However, the morphology of the diamond crystallites does change as the alcohol molecular group becomes larger. Using methanol or ethanol, the crystallites growing from the nucleation sites are composed of individual diamond crystals some of which appear to be twinned. Using isopropanol, the crystallites growing from the nucleation sites are composed of many diamond crystals clustered about the nucleation site. Raman spectroscopy from all the samples (see Figure 1) shows a distinct 1332 cm^{-1} diamond longitudinal optical peak on a broad background which is centered around 1500 cm^{-1}. Figure 2 shows the Raman spectra for the water/methanol, water/ethanol, water/isopropanol growths.

In addition to polycrystalline growth on Si(100) substrates, homoepitaxial growth on a natural Type IA diamond (100) substrate was accomplished using an equivalent water/ethanol mixture a the one used for the polycrystalline growth. Figure 3 shows the Raman spectrum along with a SEM showing the surface topography. Unlike the polycrystalline deposition, the Raman spectrum from the homoepitaxial deposition did not exhibit any scattering from the 1500 cm^{-1} non-diamond material. The full-width-half-maximum (FWHM) of the homoepitaxial layer, as determined using micro-Raman focused on the epitaxial layer, is 2.60 cm^{-1}. Examination of the bulk substrate by performing micro-Raman on the opposite substrate face from the epitaxial layer found the

FWHM of the bulk material to be 2.75 cm^{-1}. Hence, the homoepitaxial growth using water/ethanol produced a diamond epitaxial layer of apparently higher structural perfection than the starting natural diamond crystal.

This work clearly demonstrates that water-vapor discharges can promote diamond growth. Attempts to grow diamond with only methanol vapor admitted to the reactor resulted in poor nucleation and growth. Facetting was not observed on any of these diamond particles grown with only methanol. These results contrast the results of Buck et al.[14] where microwave discharges of pure methanol deposited well-factted diamond. Conversely, attempts to deposit diamond with only water vapor admitted to the reactor (in attempt to grow by chemical vapor transport from carbon on the graphite susceptor) resulted in no deposition. The water vapor discharges contribute both OH and H radicals to the growth environment. Obviously, the activation or production of atomic hydrogen in the water vapor and in the molecular H_2 processes will be different. We have no way to *in situ* measure the relative production of atomic hydrogen in these processes; however, we can measure the relative dissolution rates of solid graphite for the two processes by measuring dimensional changes on the graphite susceptor. The water process at 1000 W and 1 Torr etches graphite at approximately 25 μm/hr as compared to 5μm/hr for the H_2 process at 2000 W and 5 Torr. Hence, it is observed that the water process at lower pressure and lower power produces a much higher graphite etch rate. Despite this higher gasiphication rate, no chemical vapor transport growth is observed. Alcohol must be added to the water for diamond growth to occur.

The authors cannot dismiss the possibility that the water vapor discharge is merely a hydrogen source and that the role of OH in diamond deposition is minor. However, growth of diamond in the same reactor using H_2 - CH_4 rf discharges produces high quality diamond but only at much higher pressures and higher power levels. Typically, 5.0 Torr and 2500 W of rf power input are necessary for well-facetted crystallites when 1% CH_4 in H_2 discharges are used. Furthermore, in the H_2 - CH_4 rf discharges, the ratio of carbon to hydrogen in the gas phase is small, typically less than 2% for high quality diamond growth. Using the vapor pressures of water and methanol, the ratio of carbon to hydrogen to oxygen in this process is calculated to be 1:6:2. Emission spectra from water-alcohol discharges are dominated by emissions from the atomic hydrogen Balmer series. In addition, OH emission is observed. Emission from atomic O was not observed.

In conclusion, we have demonstrated the growth of polycrystalline diamond films from rf-plasma discharges containing water and alcohol vapors. Characterization of the films by SEM shows the films to be well faceted with the choice of alcohol effecting the nucleation density and the crystal habit. Characterization of the films by Raman spectroscopy shows the polycrystalline films to be diamond with some non-diamond bonding. Raman spectroscopy shows the single crystalline homoepitaxial films to have a FWHM of 2.60 cm^{-1} which is narrower than the starting natural crystal whose FWHM was 2.75 cm^{-1}. This technique represents a remarkable new way to manufacture diamond films through the use of non-corrosive, non-explosive, and relatively inexpensive sources. Design and implementation of growth systems using water-based processes

should be straightforward and should avoid the complexities, the safety hazards, and the expense of H_2 or halogen gas processing. The reduced pressure, reduced temperature, and reduced power density make the water-based diamond deposition technique applicable for large area diamond deposition.

References

1. B. Derjaguin and V. Fedoseev, Russ. Chem. Rev. 39, 783 (1970).

2. B.V. Spitsyn, L.L. Bouilov, and B.V. Derjaguin, J. Cryst. Growth 52, 219 (1981).

3. S. Matsumoto, Y. Sato, M. Kamo, and N. Setaka, Jpn. J. Appl. Phys. 21, 183 (1982).

4. Y. Hirose and Y. Teresawa, Jpn. J. Appl. Phys. 25, L51 (1986).

5. M. Nakazawa, T. Nakashima, and S. Seikai, Appl. Phys. Lett. 45, 823 (1984).

6. M. Kamo, Y. Sato, S. Matsumoto, and N. Setaka, J. Cryst. Growth 62, 642 (1983).

7. S. Matsumoto, M. Hiro, and T. Kobayashi, Appl. Phys. Lett. 51, 737 (1987).

8. K. Kurihara, K. Sasaki, M. Kawarada, and N. Koshiro, Appl. Phys. Lett. 52, 437 (1988).

9. L.M. Hanssen, W.A. Carrington, J.E. Butler, and K.A. Snail, Mater. Letters 7, 289 (1988).

10. G. Janssen, W.J.P. Van Enckevort, J.J.D. Schaminee, W. Vollenberg, L.J. Giling, M. Seal, J. Cryst. Growth 104, 752 (1990).

11. Peter K. Bachmann, Dieter Leers, and Hans Lydtin, Diamond and Related Materials 1, 1 (1991).

12 D.E. Rosner and J.P. Strakey, J. Phys. Chem. 77, 690 (1973).

13. M. Buck, T.J. Chuang, J.H. Kaufman, and H. Seki, Mat. Res. Soc. Symp. Proc. 162, 97 (1990).

14. J.A. Mucha, D.L. Flamm, and D.E. Ibbotson, J. Appl. Phys. 65, 3448 (1989).

15. C.F. Chen, T. M. Hon and C.L. Lin, presented at 18th Int. Conf. on Metallurgical Coatings and Thin Films (ICMCTF), San Diego, CA, April 23, 1991.

16. Yukio Saito, Kouji Sato, Hideaki Tanaka, Kazunori Fujita, Shinpei Matuda, J. Mater. Sci. 23, 842 (1988).

17. Yukio Saito, Kouji Sato, Kenichi Gomi, Hiroshi Miyadera, J. Mater. Sci. 25, 1246 (1990).

18. R.A. Rudder, G.C. Hudson, R.C. Hendry, R.E. Thomas, J.B. Posthill, and R.J. Markunas, "Applications of Diamond Films and

Related Materials", Materials Science Monograph 73, 395 (1991).

19.   R.A. Rudder, G.C. Hudson, D.P. Malta, J.B. Posthill, R.E.

Thomas, and R.J. Markunas, "Applications of Diamond Films and

Related Materials", Materials Science Monograph 73, 583 (1991).

Figure Captions

Figure 1. SEM micrographs of the polycrystalline deposits on Si(100) obtained using water/methanol, water/ethanol, and water/isopropanol.

Figure 2. Raman spectra from the polycrystalline deposits on Si(100) obtained using water/methanol, water/ethanol, and water/isopropanol.
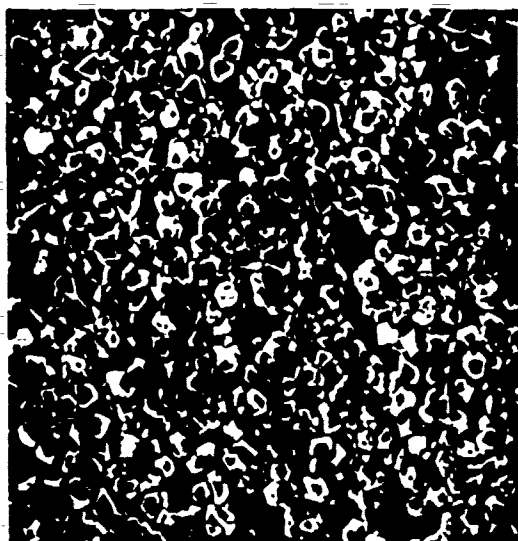
Figure 3. Raman spectrum and SEM micrograph from the homoepitaxial layer deposited using water/ethanol.
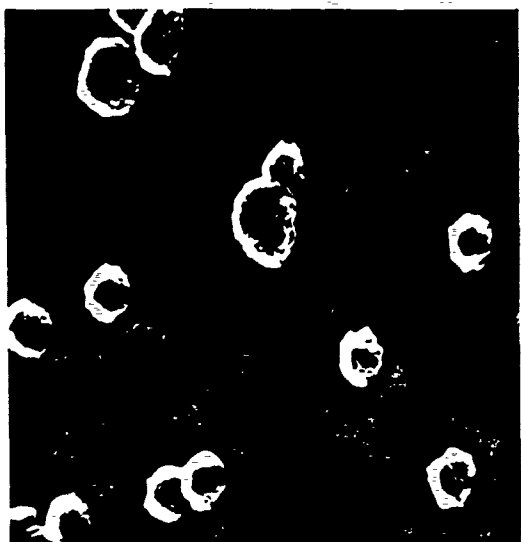
Isopropanol In Water

Ethanol In Water

Methanol In Water

Diamond Growth from Water-Alcohol Discharge

1332 cm⁻¹

FWHM ~ 2.6 cm⁻¹

Before Growth   15 μm

After Growth   15 μm

Arbitrary Units

Wavenumber (cm⁻¹)

1280.0   1440.0   1600.0   1760.0   1800.0